

1 **Dual targeting of MAPK and PI3K pathways unlocks redifferentiation of *Braf*-**
2 **mutated thyroid cancer organoids**

3

4 Hélène Lasolle ¹, Andrea Schiavo ¹, Adrien Tourneur¹, Pierre Gillotay ¹, Bárbara de Faria
5 da Fonseca ¹, Lucieli Ceolin ^{1, 2}, Olivier Monestier ¹, Benilda Aganahi ¹, Laura Chomette
6 ¹, Marina Malta Letro Kizys ¹, Lieven Haenebalcke ³, Tim Pieters ^{3, 4}, Steven Goossens
7 ^{3, 5}, Jody Haigh ⁶, Vincent Detours ¹, Ana Luiza Silva Maia ², Sabine Costagliola ¹ and
8 Mírian Romitti ^{1*}

9

10 ¹ Institut de Recherche Interdisciplinaire en Biologie Humaine et Moléculaire (IRIBHM),
11 Université Libre de Bruxelles (ULB), Brussels, Belgium

12 ² Thyroid Section, Endocrine Division, Hospital de Clínicas de Porto Alegre (HCPA),
13 Universidade Federal do Rio Grande do Sul (UFRGS), Porto Alegre, Brazil

14 ³ VIB, Flanders Institute for Biotechnology, Ghent University, Ghent, Belgium

15 ⁴ Department of Biomolecular Medicine, Faculty of Medicine and Health Sciences, Ghent
16 University, Ghent, Belgium

17 ⁵ Department of Diagnostic Sciences, Faculty of Medicine and Health Sciences, Ghent
18 University, Ghent, Belgium

19 ⁶ CancerCare Manitoba Research Institute, Department of Pharmacology and
20 Therapeutics, Rady Faculty of Health Sciences, University of Manitoba, Winnipeg,
21 Manitoba, Canada

22

23 * Corresponding author: mirian.romitti@ulb.be

24

25 The authors declare no potential conflicts of interest

26 Thyroid cancer is the most common endocrine malignancy and several genetic events
27 have been described to promote the development of thyroid carcinogenesis. Besides the
28 effects of specific mutations on thyroid cancer development, the molecular mechanisms
29 controlling tumorigenesis, tumor behavior, and drug resistance are still largely unknown.
30 Cancer organoids have been proposed as a powerful tool to study aspects related to tumor
31 development and progression and appear promising to test individual responses to
32 therapies. Here, using mESC-derived thyroid organoids, we developed a *Braf*^{V637E}-
33 inducible model able to recapitulate the features of papillary thyroid cancer *in vitro*.
34 Overexpression of the murine *Braf*^{V637E} mutation, equivalent to *Braf*^{V600E} in humans,
35 rapidly triggers to MAPK activation, cell dedifferentiation, and disruption of follicular
36 organization. *Braf*^{V637E}-expressing organoids show a transcriptomic signature for p53,
37 focal adhesion, ECM-receptor interactions, EMT, and inflammatory signaling pathways.
38 Finally, PTC-like thyroid organoids were used for drug screening assays. The
39 combination of MAPK and PI3K inhibitors reversed *Braf*^{V637E} oncogene-promoted cell
40 dedifferentiation while restoring thyroid follicle organization and function *in vitro*. Our
41 results demonstrate that pluripotent stem cells-derived thyroid cancer organoids can
42 mimic tumor development and features while providing an efficient tool for testing novel
43 targeted therapies.

44

45 INTRODUCTION

46 Pluripotent Stem Cells (PSCs) emerged as a model to dissect and recapitulate the
47 molecular events and gene networks that regulate cell fate determination, cell
48 differentiation and organogenesis. Guided differentiation of PSCs into 3D organized
49 tissue by inducible overexpression of specific transcription or growth factors and
50 inhibitors allows the derivation of *in vitro* organoids and the understanding of

51 mechanisms regulating cell differentiation and tissue formation¹. Due to their remarkable
52 self-organizing structures and functional properties, organoid technology became a
53 powerful tool to model organ development and disease ‘in a dish’^{2,3}.

54 Our group has demonstrated the generation of functional thyroid organoids
55 derived from mouse and human embryonic stem cells (mESC and hESC)^{4,5}. The
56 differentiation protocols rely on transient induction of *Nkx2.1* and *Pax8* thyroid
57 transcription factors. This approach enables an efficient generation of thyroid follicular
58 cells that organize into three-dimensional follicular structures capable of thyroid hormone
59 production *in vitro* and *in vivo*. These models, along with the further development of
60 thyroid organoids derived from healthy murine and human pluripotent or adult stem cells,
61 (PSCs/aSC)^{6–16} open new perspectives to explore thyroid developmental and pathological
62 processes, including thyroid cancer.

63 In the last decade, the use of organoids for cancer research emerged opening new
64 possibilities to better understand tumor behavior. Initially, colon, prostate, pancreatic,
65 ovarian, lung and thyroid cancer-derived organoids have been efficiently generated,
66 which resemble phenotypically and genetically the tumor of origin^{17–26}. A large set of
67 healthy and tumour-matching organoids has been generated and is available through
68 biobanks. These patient-derived organoids are particularly interesting in testing
69 individual responses to therapies^{21,26,27}.

70 Recently, studies have reported the generation of cancer models arising from
71 healthy (aSCs and PSCs) cells by controlling oncogene expression^{28–30}. By using shRNA
72 and CRISPR-Cas9, stomach cancer (*Cdh1*^{-/-}; *Tp53*^{-/-})³¹, colon cancer (*APC*, *TP53*, *KRAS*
73 and *Smad4* mutations)^{28,29,32}, pancreatic cancer (*KRAS* and/or *TP53* mutations)^{17,33} and
74 lung adenocarcinoma organoids (*HER2* overexpression) could be efficiently generated³⁰.
75 Compared to patient-derived organoids, healthy stem cells-derived cancer organoids are

76 suitable to address additional questions such as precise effects of oncogenes and early
77 events driving tumorigenesis; the role of cancer stem cells on tumor induction, genomic
78 stability, the effect of treatments at different stages of carcinogenesis and screening for
79 new therapeutical tools³⁴. Besides, they allow multiple reproducible experiments free
80 from inter-individual variability.

81 Thyroid cancer is the most frequent endocrine malignancy, and several genetic
82 events have been described as driving thyroid carcinogenesis. Papillary thyroid
83 carcinoma (PTC) is the most common malignant thyroid tumor³⁵, and aberrant activation
84 of the MAPK pathway is a hallmark³⁶. The BRAF^{V600E} mutation is the most frequent
85 genetic event, accounting for around 50% of PTCs³⁷⁻³⁹ and results in an oncogenic protein
86 with markedly elevated kinase activity that constitutively induces MEK/ERK signaling
87 transduction⁴⁰⁻⁴².

88 *BRAF*-mutated thyroid tumors are often less differentiated, mainly due to the
89 lower expression levels of thyroid functional genes *NIS*, *TSHR*, *TG* or *TPO*, leading to a
90 low Thyroid Differentiation Score (TDS)⁴³. This dedifferentiated state is associated with
91 a worse clinical condition and with a higher rate of radioactive iodine (RAI) refractory
92 tumors^{44,45}. However, its impact on prognosis is still uncertain, as BRAF^{V600E} alone has
93 not been proven to be an independent prognostic factor^{46,47}. On the other hand, *BRAF* and
94 *TERT* promoter mutated tumors are associated with higher specific mortality⁴⁸. Also,
95 studies have shown a small proportion (around 20%) of BRAF^{V600E} mutated tumors
96 presenting a higher level of differentiation associated with less aggressive behavior and
97 a preserved RAI uptake ability^{43,49}. This suggests a possible cell heterogeneity among the
98 BRAF^{V600E}-mutated tumors.

99 So far, efficient, fast, and cost-effective tools are lacking to functionally
100 characterize a large set of candidate genes in the context of thyroid carcinogenesis.

101 Thyroid cancer organoids/spheroids models have been recently described based on
102 patient tumor-derived models⁵⁰⁻⁵⁴. Tumor-derived organoids can be used to explore
103 patient-specific tumor behavior and the treatment response, but present high
104 heterogeneity and low reproducibility. Saito et al. described a mouse model of poorly
105 differentiated thyroid carcinoma obtained after transplantation of thyroid organoids
106 derived from *Tp53^{-/-}* mice with *NRAS* activating mutation²⁵. Recently, Veschi *et al.*⁵⁵
107 generated PTC and FTC organoids by inducing *BRAF*, *NRAS* and *TP53* mutations in
108 thyroid progenitors derived from hESC. After transplantation, the tumors resembled
109 Papillary and Follicular tumors and, transcriptomics analysis suggested a cooperative
110 effect of Kisspeptin receptor (KISS1R) and Tissue Inhibitor of Metalloproteinase 1
111 (TIMP1)/Matrix metallopeptidase 9 (MMP9)/Cluster of differentiation 44 (CD44), on
112 tumor development and progression⁵⁵.

113 In this study, we have established an *in vitro* organoid model for PTC to streamline
114 the process of screening potential targets and pharmaceutical agents. We achieved this by
115 leveraging our established model of thyroid generation, which involves the inducible
116 expression of the *Braf^{V637E}* mutation in functional thyroid follicles derived from mouse
117 ESCs.

118

119 RESULTS

120 mESC_BRAF^{V637E} cell line generation and characterization

121 We combined the previously described mESC transient induction thyroid differentiation
122 strategy⁴ with a *Braf^{V637E}*-ERT² inducible model⁵⁶ to generate a double-inducible
123 recombinant mESC_Braf^{V637E} cell line. The murine *Braf^{V637E}* mutation corresponds to the
124 human *Braf^{V600E}* mutation. The resulting mESC_Nkx2-1/Pax8_bTg_Braf^{V637E}_ERT²
125 clones were initially selected and characterized by the response to doxycycline (Dox)

126 treatment, confirmed by the overexpression of *Nkx2-1* and *Pax8*; and ability to
127 spontaneously differentiate into cells from the three germ-layers (Supplementary Fig. 1A-
128 C). In addition, a control mESC line was generated in which *Braf*^{V637E}_ERT² system was
129 replaced by the eGFP sequence (mESC_Nkx2-1/Pax8_bTg_eGFP). Similarly, the control
130 line responded properly to Dox induction and maintained the pluripotency capacity
131 (Supplementary Fig. 1D-F).

132

133 **Thyroid differentiation protocol**

134 The capability of the new cell line to generate thyroid follicles and express the *Braf*^{V637E}
135 oncogene was demonstrated following the mESC thyroid differentiation protocol^{4,57,58}.
136 Since we used a newly modified mESC line, the steps of the differentiation protocol were
137 tested and adapted accordingly (Fig. 1A). Here, using the mESC_Nkx2-
138 1/Pax8_bTg_Braf^{V637E} line, we observed that Dox stimulation for 5 days leads to higher
139 exogenous and endogenous *Nkx2-1*, *Pax8* and *Tg* mRNA compared to 3 or 4 days of
140 treatment (Supplementary Fig. 2A-D). Similar results were obtained using the control
141 mESC line (data not shown). Next, two weeks of treatment with cAMP (from day 9 to
142 23) markedly induced the expression levels of *Nkx2-1*, *Pax8*, *Tg*, *TshR*, *Nis*, *Tpo* and
143 exogenous *Braf*^{V637E} when compared to the control (-Dox -cAMP) (Fig. 1B).
144 Immunofluorescence staining also showed *Nkx2-1* and *Tg*-expressing cells (Fig. 1C)
145 organized into follicular structures with intraluminal iodinated-Tg (Tg-I) accumulation
146 (Fig. 1D). Since our protocol also generates other cell types than thyroid⁵⁸, a follicle
147 enrichment (FE) step was added to the protocol to enrich the follicular structures and
148 induce the *Braf*^{V637E} oncogene in a purer population. This protocol led to an increase in
149 thyroid markers levels (Fig. 1E) when compared to the non-enriched control condition
150 (No FE), while the follicular structures and functionality were preserved as demonstrated

151 by Nkx2-1, Nis and Tg-I stainings (Fig. 1F-G). Notably, after re-embedding in Matrigel
152 (MTG), follicles could be maintained in culture for at least 28 additional days without
153 major histological changes (data not shown).

154

155 **Braf^{V637E} induction on thyroid organoids leads to PTC-like phenotype**

156 To ensure that Braf^{V637E} oncogene is expressed specifically among follicular thyroid cells,
157 we used the bovine Tg (bTg) as a promoter controlling Braf^{V637E}_ERT² expression.
158 Effectively, exogenous *Braf^{V637E}* mRNA expression was rapidly induced after Dox
159 treatment (Day 9; Supplementary Fig. 2E), maintaining the expression levels stable over
160 time (Fig. 1B and Supplementary Fig. 3A), while *Tg* expression increased following the
161 differentiation program (Supplementary Fig. 3A). In the absence of tamoxifen (4OHT)
162 Braf^{V637E} protein is not active/phosphorylated since it is maintained in the nucleus in an
163 inactive complex with HSP90. The addition of 4OHT induces nuclear translocation of the
164 Braf^{V637E} mutant to the cytoplasm (NES signal)⁵⁶, then driving MAPK activation⁵⁶ (Fig.
165 2A). Indeed, 48 hours after 4OHT addition, we observed an increase in ERK
166 phosphorylation (pERK) compared to the control condition (cAMP) (Fig. 2B).

167 One of the hallmarks of thyroid cancer is the downregulation of thyroid
168 differentiation markers^{41,59}. In our organoid model, the activation of Braf^{V637E} rapidly led
169 to a progressive time-dependent decrease of *Tpo*, *TSHR* and *Tg* mRNA expression (Fig.
170 2C-E and Supplementary Fig. 3B), detected as early as 6 hours after 4OHT addition (Fig.
171 2C). Notably, more significant downregulation compared to the cAMP control was
172 observed after 48 hours and 7 days while maintained for at least 21 days (Fig. 2D-F,
173 respectively). As for PTCs, in our model, the expression of thyroid transcription factors
174 *Pax8* and *Nkx2-1* was also globally maintained. However, a partial decrease of *Nkx2.1*
175 levels was observed at 7 days, which corroborates recent findings suggesting that thyroid

176 cells transiently downregulated NKX2.1 in early tumor stages⁶⁰. Conversely, Galectin 3
177 (*Lgals3*) expression, which has been suggested as a marker for thyroid malignancies and,
178 more specifically, for PTC⁶¹, was significantly increased at 48 h and 7 days of 4OHT
179 treatment (Fig. 2D-E). Also, an increase in Fibronectin 1 (*Fnl*) expression, associated
180 with aggressive thyroid cancer^{62,63}, was observed after 7 days of *Braf*^{V637E} induction,
181 suggesting a more advanced dedifferentiated cell state in our organoid model (Fig. 2E).
182 The generation of thyroid organoids was equally successful when differentiating
183 mESC_Nkx2-1/Pax8_bTg_Braf^{V637E}_ERT2 cells using hrTSH instead of cAMP, as
184 demonstrated in Supplementary Figure 4A and C. Furthermore, the addition of 4OHT to
185 the conditioned media (for a duration of 7 days, as illustrated in Supplementary Figure
186 4B-C) led to dedifferentiation and histological changes.

187 Cell proliferation assessment demonstrated an increased proportion of Nkx2-
188 1/BrdU+ cells within the *Braf*^{V637E}-expressing organoids (4OHT) as compared to the
189 controls (cAMP) after 7 days of treatment (Fig. 2G). Interestingly, there were no
190 observable variations in proliferation even after 21 days of 4OHT treatment (Fig. 2G).
191 Furthermore, considering that prior studies have indicated that the induction of oncogenes
192 in organoids can lead to cell death⁶⁴, our analysis of apoptosis showed no significant
193 difference in the proportions of Nkx2.1/Caspase3+ between cAMP and 4OHT-treated
194 organoids both at 7 and 21 days of 4OHT treatment (Fig. 2H). However, a notable
195 increase in the proportion of Nkx2.1/Caspase3+ cells was evident when cAMP-treated
196 organoids were exposed for 24h to staurosporine, a highly potent inducer of apoptosis.
197 (Fig. 2H). Given that tumor growth arrest and antiapoptotic phenotype are linked to
198 oncogene-induced senescence (OIS)^{65,66}, we examined p21 expression at both 7 and 21
199 days of 4OHT treatment. Notably, we observed no co-expression of p21 with Nkx2-1 in
200 either the control or 4OHT-treated thyroid organoids. However, a small proportion of

201 non-thyroid cells (Nkx2.1 negative) were positive for p21 and used as positive controls
202 (Supplementary Fig. 5A-C).

203 Histological characterization performed after 48 hours of continuous activation of
204 $\text{Braf}^{\text{V637E}}$ by 4OHT demonstrated disruption of the follicular organization in non-enriched
205 thyroid organoids compared to the control condition (cAMP) (Fig. 3A). Nkx2-1 and Tg
206 staining revealed that $\text{Braf}^{\text{V637E}}$ oncogene strongly disturbs thyroid follicles resulting in
207 elongated and unorganized structures. In addition, heterogeneous expression of Tg was
208 observed among the Nkx2-1 cells (Fig. 3A). Further analysis, performed in follicle
209 enriched (FE) population, confirmed the effect of $\text{Braf}^{\text{V637E}}$ oncogene in promoting cell
210 dedifferentiation and loss of follicle organization. Tg levels were overall reduced and
211 heterogeneous among the unorganized Nkx2-1+ cells (Fig. 3B). Interestingly, the cell
212 disorganization caused by $\text{Braf}^{\text{V637E}}$ oncogene might pass by an initial expansion of the
213 follicular size with infiltration of Nkx2-1 cells inside of the lumen compartment, which
214 also presents a heterogeneous distribution of Tg (Supplementary Fig. 3C) since this
215 feature was observed among some “follicular-like” remaining structures after 48 h of
216 4OHT treatment. Reassuringly, staining for E-Cadherin (epithelial) and Zo-1 (intra-
217 luminal) adhesion markers showed that $\text{Braf}^{\text{V637E}}$ -expressing cells are not able to preserve
218 polarization and, consequently lumen space is not well defined in most of the structures
219 (Fig. 3C and D, respectively). Therefore, the functionality of those cells was impaired
220 and, Nis expression and Tg-I accumulation were significantly reduced compared to the
221 control condition (Fig. 3E-F). Of note, despite the strong effect of $\text{Braf}^{\text{V637E}}$ oncogene on
222 thyroid follicle disruption, we observed that few follicles still preserved a certain degree
223 of organization (Supplementary Fig. 3D) after 48 h of 4OHT treatment. As expected, after
224 7 days of $\text{Braf}^{\text{V637E}}$ continuous stimulation, a higher level of cell dedifferentiation and
225 lack of organization could be detected, with a lower proportion of the Nkx2-1 cells

226 expressing Tg compared to control (cAMP) (Fig. 3G) and to the previous time point (48
227 h; Fig. 3A). However, despite the absence of proper follicular organization, there was an
228 increased proportion of Tg-expressing cells within the *Braf^{V637E}*-expressing organoids
229 after 21 days of 4OHT treatment compared to earlier time points (48 h and 7 days; Fig.
230 3H). This observation, in conjunction with the gene expression and the proliferation data
231 (Fig. 2F-G) implies a partial arrest in the tumorigenic processes at a later stage.

232 The above-described experiments were also performed using the control TRE-
233 *Nkx2-1-Pax8_bTg-eGFP* cell line. Adding 4OHT to mature follicles for 7 days did not
234 impair the levels of the thyroid differentiation markers and the follicles' organization
235 (Supplementary Fig. 6A-B). Furthermore, there was a slight increase in the proportions
236 of *Nkx2.1* and GFP-expressing cells when WT organoids were treated with 4OHT (7
237 days; Supplementary Fig. 6C). It's worth noting, as previously demonstrated⁵⁸, that
238 bTg_GFP-expressing cells do not encompass the entire Tg-expressing cells population
239 (Supplementary Fig. 6D). This could be attributed to the lack of regulatory regions not
240 included in our construct.

241

242 **Effect of transient *Braf^{V637E}*-induction on cell differentiation**

243 Since our system for *Braf^{V637E}* activation is dependent on continuous treatment with
244 4OHT, we transiently treated the cells with 4OHT for 2 days, followed by 5 days of
245 culture in a 4OHT-free medium (cAMP) in order to explore if the oncogenic effect is
246 maintained when the protein is not active. Surprisingly, we did not observe recovery in
247 *Nkx2-1*, *TSHR*, *Tg* or *Tpo* gene expression levels (Supplementary Fig. 7A, C-E) after
248 4OHT removal. However, *Pax8* and *Slc5a5/Nis* expression was partially recovered
249 (Supplementary Fig. 7B and F), confirming the specific inhibitory effect of *Braf^{V637E}*
250 oncogene on *Slc5a5/Nis* expression. These findings indicate that *Nis* regulatory

251 mechanisms are maintained in our system and suggest it as a tool for Nis-reactivation
252 studies.

253

254 **Screening for Nis re-expression using signaling pathways inhibitors**

255 Studies in mouse models and humans have demonstrated that tumors carrying *BRAF*
256 mutations show reduced expression of *Nis* and, consequently a higher rate of radioiodine
257 (RAI) refractoriness^{41,44,67}. Here, we used our organoids model to explore new strategies
258 to reactivate *Nis* expression in *Braf*^{V637E}-expressing cells by screening distinct categories
259 of inhibitors previously described to be involved in *Nis* regulation^{68,69}. PD0325901
260 (MEK inhibitor), LY204002 (PI3K inhibitor), VPA (HDAC inhibitor), NAC (N-acetyl
261 cysteine, antioxidant compound), 5-AZA-2' deoxycytidine and RG108 (DMNT
262 inhibitors) were tested isolated and/or in combination for 3 days (in addition to
263 cAMP+4OHT) using *Braf*^{V637E}-expressing organoids (previously treated for 4 days with
264 4OHT; Fig. 4A). Initially, we observed that VPA alone was the only treatment able to
265 completely restore *Nis* expression levels (Fig. 4B, C and Supplementary Fig. 8A).
266 However, when combined, PD0325901 and LY204002 inhibitors; PD0325901,
267 LY204002 and VPA; and PD0325901 and NAC resulted in a great increase of *Nis* mRNA
268 (Fig. 4B, C and Supplementary Fig. 8A). IF staining shows Nis protein re-expression
269 among *Braf*^{V637E}-induced cells treated with VPA alone, but localization was not restricted
270 to the basolateral membrane. In contrast, when cells were treated with MEK (PD) or
271 PI3K (LY) inhibitors, associated or not with VPA, we observed Nis protein correctly
272 localized at the basolateral membrane and surprisingly, it restored the follicular structure
273 (Fig. 4C).

274

275 **MAPK and PI3K signaling inhibition cause *Braf*^{V637E}-induced cell redifferentiation**
276 **and function recovery**

277 Since we observed that HDAC, MEK, and PI3K inhibition seem to favor follicle
278 reorganization, we evaluated if such treatments also induce cell redifferentiation and
279 function recovery. Initially, we analyzed the gene expression levels of thyroid
280 differentiation markers strongly affected by *Braf*^{V637E} induction. The effects of isolated
281 and combined drugs on *Tg*, *TSHR*, *Tpo*, *Nkx2-1* and *Duox* genes appear to be variable and
282 pathway-dependent (Supplementary Fig. 8B-F). As for *Slc5a5/Nis*, MEK and PI3K
283 inhibition in combination with or without VPA resulted in complete recovery of *Tg*, *TSHR*
284 and *Tpo* mRNA levels (Fig. 4D-F), indicating cell redifferentiation. While *TSHR* levels
285 can be restored by treatment with isolated inhibitors (Fig. 4E), *Tpo* expression appears to
286 be dependent on PI3K signaling (Fig. 4F). On the other hand, *Tg* mRNA expression was
287 recovered only when the inhibitors were used in combination (Fig. 4D). Indeed,
288 immunostaining showed that isolated inhibitors could not restore Tg levels. Nevertheless,
289 a higher proportion of Tg-expressing cells was observed with the MEK inhibitor
290 PD0325901 (Supplementary Fig. 8G). Conversely, combined MEK and PI3K inhibitors
291 restored Tg protein levels and led to a significant reorganization of the cells into follicles
292 comparable to the control (cAMP) condition (Fig. 4G-H). Considering that inhibition of
293 MEK and PI3K pathways (+/-VPA) recovered thyroid differentiation and follicular
294 organization, we tested the functionality of reorganized follicles. Remarkably, we
295 observed an accumulation of Tg-I in the lumen of follicles treated with the combinations
296 of inhibitors (Fig. 4I). The organification assay confirmed that the co-treatment restored
297 iodide uptake and ¹²⁵I binding to proteins resulting in organification levels comparable to
298 the control (Fig. 4J-L).

299

300 **Dabrafenib and trametinib effect on redifferentiation is potentialized by PI3K**

301 **inhibition**

302 The treatment of advanced thyroid carcinomas as PDTC and ATC with BRAF inhibitor
303 dabrafenib and MEK inhibitor trametinib have shown significant redifferentiation and
304 response rates in *BRAF*-mutated tumors⁷⁰⁻⁷². In this study, we examined the effect of
305 isolated dabrafenib and trametinib inhibitors, as well as their combination with PI3K
306 inhibition, on thyroid cancer organoids. Using the same experimental approach (Fig. 4A),
307 we noted that both dabrafenib and trametinib treatments successfully restored *Nis*
308 expression to levels comparable to the control group (treated with cAMP). Notably, the
309 combination of trametinib with a PI3K inhibitor yielded an even more significant
310 recovery, resulting in a threefold increase compared to the control group (Fig. 5A).
311 Furthermore, isolated treatments with dabrafenib and trametinib elicited a moderate
312 restoration of the main thyroid differentiation markers' expression. However, the most
313 substantial recovery of *Tg*, *Tpo*, and *TSHR* levels was observed when organoids were
314 subjected to a combination of dabrafenib and trametinib along with a PI3K inhibitor, with
315 the latter showing the most pronounced effect (Fig. 5B-D). Interestingly, both *Tg* and *Nis*
316 proteins were detectable in all experimental conditions, with some cells organized into
317 functional follicles able to produce *Tg*-I (Fig. 5E). However, due to the complexity of the
318 cell composition and organization of our 3D organoids, accurately quantifying the
319 proportion of reorganized follicles proved to be very challenging and could not be
320 efficiently assessed in the present study. Furthermore, our proliferation and apoptosis
321 assays revealed that co-treatment with Trametinib and LY led to a decrease in
322 proliferation (Nkx2.1/BrdU+ cells) and a marginal increase in apoptosis (Nkx2.1/Caspase
323 3 + cells). Comparable outcomes were achieved through incubation with MEK and PI3K
324 inhibitors (PD+LY). Nevertheless, it's worth noting that apoptosis induction was notably

325 more pronounced when compared to the effects observed with Trametinib+LY treatment
326 (Fig. 5F-G). Western blot analysis distinctly revealed an increase in pERK levels after a
327 7-day 4OHT treatment. However, when Trametinib and LY were combined in the
328 treatment, it led to a mild inhibition of pERK compared to the conditions involving 4OHT
329 alone or in combination with PD+LY (Fig. 5H).

330

331 **Transcriptomic characterization of the PTC model and drug screening**

332 Transcriptomic analysis of control (cAMP), $\text{Braf}^{\text{V637E}}$ -induced (4OHT) and inhibitors-
333 treated (PD+LY) organoids (Fig. 6A) confirmed downregulation of thyroid genes under
334 $\text{Braf}^{\text{V637E}}$ stimulation (4OHT condition) whereas, global recovery of expression was
335 observed under inhibitors treatment (Fig. 6A). Accordingly, thyroid differentiation scores
336 (TDS and enhanced (e)TDS) were decreased under $\text{Braf}^{\text{V637E}}$ induction while they
337 recovered in the presence of inhibitors (Fig. 6B). Conversely, the ERK activation score
338 was higher in the $\text{Braf}^{\text{V637E}}$ samples and decreased sharply under inhibitor conditions (Fig.
339 6C). Since bulk RNAseq was performed using the follicle-enriched population, the
340 presence of non-thyroid cells is reduced compared with the whole original organoids but
341 still present. It may explain the modest increase in ERK score among $\text{Braf}^{\text{V637E}}$ -activated
342 cells while the apparent decrease under the condition with inhibitors reflects the effect of
343 the treatment on each cell type.

344 Differential expression analysis identified 321 Differential Expressed Genes
345 (DEGs; 156 upregulated and 165 downregulated genes) in the 4OHT condition compared
346 to cAMP; and 853 DEGs in inhibitors compared to 4OHT (287 upregulated and 566
347 downregulated genes). Gene enrichment classification analysis of DEGs results is
348 presented in Fig. 6D-G. Briefly, among the upregulated genes in $\text{Braf}^{\text{V637E}}$ -induced
349 compared to control, we observed gene signature for the hyperactivation of PI3K-AKT-

350 mTOR, TNF, and cytokines signaling and promotion of Epithelial-Mesenchymal
351 transition (EMT) (Fig. 6D). While genes associated with thyroid hormone production,
352 TGF-beta, Wnt/Beta-Catenin pathway, and regulation of angiogenesis were down-
353 regulated (Fig. 6E). Conversely, the inhibitor's treatment, compared to 4OHT condition,
354 evidenced upregulation of genes associated with thyroid hormone production, cell-cell
355 contact, extra-cellular matrix organization, and angiogenesis processes (Fig. 6F), while
356 PI3K, MAPK, TNF, cytokines signaling, ECM-receptor interactions and EMT-related
357 genes were downregulated (Fig. 6G). The list of the DEGs for each gene enrichment
358 classification is provided in Supplementary Table 4.

359 Given our transcriptomics analysis, which indicated elevated expression of
360 inflammation-related genes and downregulation of the Wnt/β-catenin pathway in
361 *Braf*^{V637E}-expressing cells, we tested the effect of anti-inflammatory drugs, specifically
362 dexamethasone and CC-5013 (Lenalidomide; TNF-alpha inhibitor) as well as CHIR-
363 99021 (Wnt/β-catenin activator) on our cancer organoids. Following the same
364 experimental strategy as with the other inhibitors (Fig. 4A), we observed that co-treatment
365 with dexamethasone and CC-5013 led to approximately a 3.5 fold increase in *Nis*
366 expression compared to the control condition (cAMP) (Supplementary Fig. 9A),
367 confirming the previously described inhibitory effect of inflammation on *Nis* expression.
368 On the other hand, for the other main thyroid differentiation genes, namely *Tg*, *TSHR* and
369 *Tpo*, treatment with anti-inflammatory drugs and the Wnt/β-catenin activator did not
370 result in their re-expression (Supplementary Fig. 9B-D). This suggests that these
371 alterations are likely a consequence of the oncogenic process rather than being driving
372 factors.

373

374

375 **DISCUSSION**

376 Here, we described a *Braf*^{V637E} oncogene-derived thyroid cancer organoid model
377 recapitulating patient tumor features. *In vitro* thyroid cancer models that recapitulate
378 tumor development and behavior can facilitate the identification of early tumor drivers
379 and enable the screening of several new drugs for the treatment of thyroid cancer without
380 the need to use too many animal models. Combining our previous thyroid organoid model
381 derived from mESCs with an inducible system, the *Braf*^{V637E} oncogene could be induced
382 explicitly in mature Tg-expressing cells to obtain a 3D *in vitro* cancer model.
383 Overexpression of *Braf*^{V637E} rapidly led to MAPK activation with increased pERK, cell
384 dedifferentiation, and disruption of follicular organization. Similar effects have been
385 described in genetically modified mouse models^{41,59,73}. Furthermore, the gene expression
386 signature of our cancer organoids confirmed the findings found in the PTC samples,
387 which also showed enrichment of genes associated to p53, focal adhesion, ECM-receptor
388 interactions, EMT and inflammatory pathways^{74–76}.

389 Activating mutations in the *BRAF* gene are found in approximately 7% of all solid
390 human tumors, particularly common in PTCs, ATCs, and melanomas. In addition, they
391 have been reported less frequently in colorectal cancers (CRCs), lung cancers, pediatric
392 low-grade gliomas (PLGGs), glioblastomas, breast cancers, and serous ovarian cancers^{77–}
393 ⁸³. In PTCs and melanomas, *BRAF*^{V600E} mutation seems to be associated with a higher
394 degree of dedifferentiation and more aggressive histological patterns. However, its
395 prognostic role is still debated as it was not found independently of histological
396 features^{46,47}. Nevertheless, studies suggest that *BRAF*^{V600E} might predict response to
397 tyrosine kinase inhibitors (TKIs) in melanoma and lung cancer^{84,85}.

398 Surgery remains the first choice for thyroid cancer therapy. Recommended post-
399 operative treatment includes TSH suppression and RAI ablation, particularly as adjuvant

400 treatment for patients at high risk for tumor recurrence and to treat patients with
401 persistent/recurrent or metastatic disease⁸⁶. The benefit of RAI has been demonstrated in
402 patients by reducing the risk of recurrence and disease-related mortality⁸⁷. However,
403 approximately two-thirds of metastatic DTC become radioiodine refractory (RR-DTC),
404 defined by the absence of iodine uptake or tumor progression despite uptake^{88,89}. There
405 is no curative treatment for radioiodine refractory DTCs. The recommended first-line
406 systemic treatment when local therapies are not possible is targeted therapies using
407 mainly multitarget TKIs, such as Lenvatinib showed a progression-free survival of 18
408 months^{67,90–92}.

409 NIS, a basal membrane iodide transporter, plays a critical role in radioiodine
410 accumulation in DTC cells and its level is closely related to response to RAI (I^{131}) therapy.
411 Studies in mouse models and humans have shown that the presence of *BRAF* mutations
412 results in lower *Nis* levels and, consequently a higher rate of RAI-refractory tumours^{41,44}.
413 Here, we confirmed that this regulation is preserved in our cancer organoids, as disruption
414 of *Braf*^{V637E} activation led to in recovery of *Nis* levels. As TKIs, retinoic acids (RA),
415 histone deacetylase inhibitors (HDAC), peroxisome proliferator-activated receptor-
416 gamma (PPARG) have been tested to promote redifferentiation and *NIS* re-expression of
417 RR-DTCs, to suggest RAI treatment after a short, targeted treatment^{90,93–95}. This strategy
418 could lead to tumor response while limiting adverse effects and, several clinical trials are
419 ongoing. However, the re-expression of NIS is insufficient to explain the response to
420 redifferentiation therapeutics and RAI treatment. Membrane trafficking and the cellular
421 machinery that concentrate and retain iodine must be preserved⁹⁶ in a follicular
422 organization. Our model is proving to be a potential tool for redifferentiation studies
423 because of its ability to test large sets and combinations of treatments and to assess
424 follicular reorganization and iodide organification capacity using a functional assay that

425 is likely to be more strongly associated with response to RAI treatment than *NIS* mRNA
426 levels. *Braf*^{V637E}-expressing cells treated with VPA, MAPK, PI3K, Dabrafenib,
427 Trametinib, and inflammation inhibitors were shown to restore the expression of *Nis*.
428 Interestingly, the combination of MAPK (BRAF and MEK) and PI3K inhibitors also
429 promoted the restoration of thyroid markers, follicular organization, and iodide
430 organification ability. Interestingly, an ongoing clinical trial tests the effect of BKM120,
431 a PI3K inhibitor, in patients with progressive, metastatic, refractory, follicular or poorly
432 differentiated thyroid cancers (NCT01830504). However, the association with MAPK
433 inhibitors is still not evaluated in patients with thyroid cancer.

434 In *BRAF*-mutated tumors, studies have shown that the combination of TKIs
435 therapies appears more effective and circumvents primary and acquired resistance to TKI
436 therapy. Often, resistance is due to reactivation of the MAPK/ERK pathway or activation
437 of other signaling pathways such as PTEN, NF-1 or RAS. It may also result from the
438 hyperactivation of tyrosine kinase receptors, such as PDFR β , IGF-1R and HGF, which
439 lead to activation of the AKT/PI3K pathway⁹⁷. Studies in patients with advanced
440 melanoma carrying a *BRAF*^{V600E} mutation have shown that combining BRAF and MEK
441 inhibitors resulted in a higher rate of complete/partial responses and median progression-
442 free survival compared with monotherapy groups^{98–100}. Such significant results lead to
443 the use of drug combinations as standard treatment for patients^{101,102}. Likewise, phase II
444 clinical trials have demonstrated noteworthy response rates in advanced *BRAF*-mutated
445 thyroid carcinomas when treated with a combination of the BRAF inhibitor dabrafenib
446 and MEK inhibitor trametinib⁷⁰. Furthermore, recent findings have shown that the
447 administration of dabrafenib-trametinib treatment followed by surgery can yield 24-
448 month overall survival (OS) rates as high as 80% in ATCs¹⁰³.

449 In summary, we have developed a *Braf*^{V637E} oncogene-expressing thyroid cancer
450 organoid *in vitro* model from mESCs that recapitulates transcriptomic and histological
451 features of PTCs at early and advanced stages. Moreover, we demonstrated that the
452 combination of MEK and PI3K inhibitors promotes *Nis* re-expression and cell re-
453 differentiation leading to the restoration of follicular structures and thyroid functionality.
454 Considering the robustness of this *in vitro* model, which allows controlled induction of
455 the major thyroid oncogene in a three-dimensional system, its efficiency and simplicity,
456 our model can be used to study mechanisms associated with thyroid cancer development
457 and progression, thyroid redifferentiation, and drug screening.

458

459 MATERIAL AND METHODS

460

461 Cell culture and mESC_Braf^{V637E} line generation

462 The previously genetically modified G4 RosaLuc mouse embryonic stem cell line
463 (mESC)¹⁰⁴ was initially cultured on gamma-irradiated mouse embryonic fibroblasts
464 (MEFs) feeder using mouse stem cell medium^{4,58} and incubated at 37 °C, 5 % CO² and
465 >95 % humidity. Cells were routinely tested for mycoplasma. To insert the target
466 sequences into the modified Rosa26 locus of G4 RosaLuc mESCs, around 1x10⁵ cells
467 were transfected using the Flpe expressing vector¹⁰⁴ and the target vector containing the
468 rtTA-TRE induction system, thyroid transcription factors, Nkx2-1 and Pax8 and bTg-
469 NES-Braf^{V637E}-ERT² sequences (Supplementary Fig. 1A) following the lipofectamine
470 3000 protocol (Thermo Scientific). The Braf^{V637E} mutation here used for mouse cells is
471 equivalent to the human BRAF^{V600E} mutation⁵⁶. Briefly, 1x10⁶ mESCs were transfected
472 (in suspension) with 20 µg of each vector and cultured on Neomycin-resistant MEFs.
473 G418 (Neomycin; 300 µg/ml) was applied 48 h after transfection, for 10 days, and

474 individual clones were isolated (colonies were separated from the MEFs using insulin
475 needles) and further expanded. Clones were screened by immunofluorescence for Nkx2-
476 1 and Pax8 expression after three days of incubation with 1 μ g/ml Doxycyclin (Dox)
477 (Supplementary Fig. 1B). Positive clones were then characterized according to
478 pluripotency maintenance (Supplementary Fig. 1C), *Nkx2-1* and *Pax8* expression, and
479 efficiency of thyroid differentiation. In addition, we generated an mESC control line
480 where the sequences of NES-BRAF^{V637E}-ERT² were replaced by the eGFP sequence,
481 resulting in the TRE-Nkx2-1-Pax8_bTg-eGFP line (Supplementary Fig. 1D). The mESC
482 control line generation, selection and characterization were performed as described above
483 (Supplementary Fig. 1E, F).

484 **Thyroid differentiation protocol**

485 G4 RosaLuc TRE-Nkx2-1-Pax8_bTg-NES-Braf^{V637E}-ERT² and TRE-Nkx2-1-
486 Pax8_bTg-eGFP cells were cultured and differentiated as described previously by
487 Antonica *et al.* (2012)⁴ with few modifications. Briefly, modified mESCs cultured in
488 mESC media on top of MEFs were split using Trypsin EDTA (TE). Then, cells were
489 resuspended in mESC media⁵⁷ and seeded into a 10-cm petri dish for 30-45 min allowing
490 the attachment of most of the MEFs. mESC-enriched supernatant was collected,
491 centrifuged (500g for 5min), and resuspended in differentiation media⁵⁷, cells were
492 counted and finally diluted to 40,000 cells/ml. Embryoid bodies (EBs), were then
493 generated by hanging drops (25 μ l drops containing 1,000 cells), collected after four days
494 and embedded in growth factor reduced Matrigel (GFR MTG; BD Biosciences); 50 μ l
495 MTG drops (containing around 20 EBs) were plated into 12-wells plates. EBs were
496 differentiated using a differentiation medium (1 ml/well) initially supplemented with
497 1 μ g/ml of Doxycycline (Sigma) for five days, followed by two weeks of maturation
498 induction by using 0.3 μ mol of 8-Br-cAMP (BioLog Life Science Institute) or 1mU ml⁻¹

499 of thyrotropin (hrTSH; Genzyme). The culture medium was changed every 2 days.
500 Thyroid differentiation and functionality were evaluated by transcriptomics (RT-PCR and
501 bulk RNA sequencing), immunofluorescence, and iodide organification.

502

503 **Braf^{V637E} induction and drug screening**

504 After full thyroid maturation (Day 23), MTG drops were washed twice with Hanks's
505 balanced salt solution (HBSS, containing calcium and magnesium; Invitrogen) and
506 incubated in a HBSS solution (1 ml per well) containing 10 U/ml of dispase II (Roche)
507 and 125 U/ml of collagenase type IV (Sigma) for 30 min at 37°C. Then the enzymes were
508 inactivated by adding 10% FBS and cells were centrifuged at 500g for 3 min. Cells were
509 rinsed twice with HBSS, and the follicle population was enriched by filtering using 30
510 µm (single cell removal) and 100 µm reverse strainer (Pluriselect). Finally, enriched
511 structures were re-embedded in GFR MTG (50µl) and plated into 12-well plates. Twenty-
512 four hours later, cells were incubated with 1 µM of 4-Hydroxytamoxifen (4OHT) (Sigma)
513 and 8-Br-cAMP or hrTSH for 24h, 48h, 7 days or 3 weeks to promote Braf^{V637E}-induced
514 phosphorylation of MAPK pathway⁵⁶. The control condition, treated with cAMP and/or
515 hrTSH, was also treated with vehicle ethanol for 4OHT treatment comparisons.

516 Braf^{V637E}-induced thyroid organoids (previously treated for four days with 4OHT) were
517 also cultured in addition to distinct compounds, previously suggested to regulate Nis re-
518 expression and inhibit Braf^{V637E} oncogenic effects^{68,69}. Among the screened drugs,
519 several cell processes were targeted by the following compounds: PD0325901 (MEK
520 inhibitor; 250nM; Stem Cell), LY204002 (PI3K inhibitor; 5µM; Selleckchem), VPA
521 (HDAC inhibitor; 250µM; Sigma), NAC (N-acetyl cysteine, antioxidant compound;
522 2mM; Sigma), 5-AZA-2' deoxycytidine (DNA methyltransferase (DMNT) inhibitor;
523 1µM; Sigma) and RG108 (DMNT inhibitor; 10µM; Sigma). Furthermore, experiments

524 were also conducted using inhibitors that are already clinically approved for the treatment
525 of thyroid cancer, namely dabrafenib (BRAF inhibitor; 100nM; Selleckchem) and/or
526 trametinib (MEK inhibitor; 20nM; Selleckchem).

527 Disrupted pathways identified by transcriptomics analysis in 4OHT condition compared
528 to cAMP control were inhibited/activated by treatment with dexamethasone (anti-
529 inflammatory drug; 50nM; Sigma), CC-5013 (Lenalidomide; TNF-alpha inhibitor;
530 10 μ M; Selleckchem) and CHIR- 99021(Wnt/ β -catenin activator; 3 μ M; Selleckchem). All
531 inhibitor treatments involved organoids that had previously been exposed to
532 cAMP+4OHT for four days, and they were subsequently subjected to continuous
533 incubation with cAMP+4OHT+inhibitors for an additional 3 days. Culture media was
534 replenished every 2 days. All experiments were performed following the same time points
535 of incubation described above.

536

537 **Flow cytometry**

538 *Proliferation assay:* Organoids subjected to various treatments, including controls
539 (cAMP), 4OHT, and 4OHT+inhibitors, at both 7 days (day 30) and 21 days (day 54),
540 were exposed to BrdU (1mM) for a duration of 3 hours. Subsequently, a proliferation
541 assay was conducted in accordance with the BrdU Flow Kit staining protocol (BD)
542 instructions. Briefly, Matrigel drops (pool of at least four replicates per condition) were
543 first digested with HBSS solution containing 10 U/ml dispase II and 125 U/ml
544 collagenase type IV for 30-60 min at 37°C; then a single cell suspension was obtained by
545 dissociation with TripLE Express (10-15 min incubation at 37°C), the enzymes were
546 inactivated by addition of differentiation medium. After centrifugation (500 g for 3 min),
547 samples were rinsed with PBS, and then the BrdU Flow Kit staining protocol (BD
548 Biosciences) was used according to the manufacturer's instructions. In order to identify

549 the BrdU incorporated cells among the thyroid population, cells were also stained using
550 primary Nkx2-1 antibody (1:100; Abcam) and donkey anti-rabbit IgG Cy3-conjugated
551 (1:300; Jackson Immunoresearch). As controls, we used cells untreated with BrdU and
552 stained with the APC anti-BrdU antibody for BrdU gating while for Nkx2.1 gating, cells
553 were incubated only with the secondary antibody. Data are presented as a percentage of
554 double-positive (BrdU/Nkx2.1) cells. For each experiment, at least four wells from each
555 condition were used.

556 *Apoptosis assay:* Organoids subjected to various treatments, including controls (cAMP),
557 4OHT, and 4OHT+inhibitors, at both 7 days (day 30) and 21 days (day 54) were collected
558 and dissociated into single cells following the protocol described above (proliferation
559 assay section). Cells were then fixed and permeabilized using the BD
560 Cytofix/Cytoperm™ Fixation/Permeabilization Kit (BD Biosciences) and stained using
561 Nkx2-1 antibody (1:100; Abcam) and donkey anti-rabbit IgG Cy3-conjugated secondary
562 antibody (1:300; Jackson Immunoresearch) combined with FITC Rabbit Anti-Active
563 Caspase-3 conjugated antibody (1:5; BD Biosciences). As a positive control, cAMP-
564 treated organoids were incubated with Staurosporine (10nM; Sigma) for 16 hours and
565 collected at the respective time points following the procedures described above.
566 Untreated cells and cells incubated only with the secondary antibody (isotype) were used
567 as negative controls for the gating strategy. For each experiment, at least four wells from
568 each condition were used.

569 *Proportion of bTg-GFP cells:* The proportions of Nkx2.1 and GFP cells in the control
570 mESC line (TRE-Nkx2-1-Pax8_bTg-eGFP) were evaluated at day 30. Controls (cAMP)
571 and 4OHT-treated (7 days) organoids were dissociated and stained for Nkx2.1 following
572 the steps described above (apoptosis assay session). GFP detection was based on the
573 endogenous expression (bTg-eGFP). Undifferentiated cells (mESCs) and cells incubated

574 only with the secondary antibody (isotype) were used as negative controls for the gating
575 strategy. For each experiment, at least four wells from each condition were used.
576 All analyses were performed using the LSR-Fortessa X-20 flow cytometer and BD
577 FACSDiva software was used for the quantification analysis. Data are presented as a
578 percentage of positive cells.

579

580 **Immunofluorescence staining**

581 Organoids embedded in MTG were fixed in 4% paraformaldehyde (PFA; Sigma) for 1 h
582 at room temperature (RT) and washed three times in PBS. Samples were either stained as
583 whole mount (MTG drop) or embedded in 4% low-melting agarose and cut using
584 Vibratome (80-100 μ m; Sigma). Blocking was performed using a solution of PBS
585 containing 3% bovine serum albumin (BSA; Sigma), 5% horse serum (Invitrogen) and
586 0.3% Triton X-100 (Sigma) for 30 min at RT. The primary and secondary antibodies were
587 diluted in a solution of PBS containing 3% BSA, 1% horse serum and 0.1% Triton X-
588 100. Primary antibodies were incubated overnight at 4°C followed by incubation with
589 secondary antibodies and Hoechst for 2 h at RT. Slides were mounted with Glycergel
590 (Dako).

591 For paraffin embedding, organoids were fixed in 4% PFA for 1 h at 4°C and kept in 70%
592 ethanol at 4°C before processing. Samples were then embedded in paraffin, sectioned (5
593 μ m), mounted on glass slides, deparaffinized, and rehydrated following standard
594 protocols. For immunostaining, antigen retrieval was performed by incubating the
595 sections for 10 min in the microwave (850 W) in Sodium Citrate Buffer (10 mM Sodium
596 Citrate, 0.05% Tween 20, pH 6.0). After cooling, the sections were rinsed with PBS and
597 blocked with 1% BSA and 10% horse serum PBS solution for 1 h at RT. Primary
598 antibodies (Supplementary Table 1) were diluted in the blocking solution and incubated

599 overnight at 4°C. The sections were rinsed three times in PBS and incubated with Hoechst
600 and secondary antibodies diluted in blocking solution for 1 h at RT. Slides were mounted
601 with Glycergel (Dako). Imaging was performed using a Zeiss LSM510 META confocal
602 microscope and a Leica DMI6000 microscope with DFC365FX camera. The antibodies
603 specifications and dilutions are listed in the supplementary Table 1.

604

605 **Western blot**

606 Follicle enriched-organoids were initially isolated (collagenase IV/dispase II solution,
607 described above) from at least 6 distinct wells and pooled together for protein extraction
608 using RIPA buffer. The protein concentration was determined according to Pierce 660
609 nm protein assay reagent protocol (Thermo Scientific). Briefly, for each sample, 30–50
610 µg of protein was fractionated by 10% SDS–PAGE and blotted onto an Immobilon PVDF
611 membrane (Millipore). Non-specific binding sites were blocked by incubation with 5%
612 BSA in Tris-buffered saline (TBS) 0.1% Tween-20 (TBS-T) for 1 h. Thereafter, the
613 membrane was incubated overnight at 4 °C with primary antibodies against phospho-
614 ERK1/2 (1:1,000; Cell Signaling), ERK1/2 (1:400; Santa Cruz Biotechnology), and β-
615 Actin (1:1,1000; Cell Signaling) in a blocking solution. Next, the membrane was
616 incubated with horseradish peroxidase-conjugated anti-rabbit (1:1,000; Cell Signaling) or
617 anti-mouse antibody (1:1,000; Cell Signaling) in a blocking solution, for 60 min at RT.
618 The antigen-antibody complexes were visualized using an enhanced chemiluminescence
619 system (GE Healthcare) and captured by Azure 500 system (Azure Biosystems).

620

621 **Iodide organification assay**

622 Thyroid organoids treated with cAMP, cAMP+4OHT, cAMP+4OHT+PD+LY and
623 cAMP+4OHT+PD+LY+VPA were tested for the ability of iodide uptake and

624 organification as previously described^{4,58}. Briefly, cells were washed with HBSS and
625 incubated with 1 ml per well of an organification medium containing 1,000,000 c.p.m.
626 per ml ¹²⁵I (PerkinElmer) and 100 nM sodium iodide (NaI, Sigma) in HBSS for 2 h at 37
627 °C. The reaction was stopped by the addition of 1 ml of methimazole (MMI; 4 mM,
628 Sigma). After two washes with cold PBS, organoids were dissociated by incubation with
629 trypsin/EDTA (Invitrogen) for 10 min at 37 °C. For iodide uptake quantification, cells
630 were collected, and radioactivity was measured using a gamma-counter. Subsequently,
631 proteins were precipitated by adding 100 µl of gamma-globulins (10 mg/ml; Sigma) and
632 2 ml of 20% TCA followed by centrifugation at 2,000 r.p.m. for 10 min, at 4°C and the
633 radioactivity of protein-bound ¹²⁵I (PBI) was measured. Iodide organification was
634 calculated as an iodide uptake/PBI ratio and, the values were expressed as a percentage.
635 Cells were also treated with 1 mM sodium perchlorate (Nis inhibitor; NaClO₄, Sigma-
636 Aldrich) and 2 mM MMI (Tpo inhibitor; Sigma-Aldrich) as iodide uptake and protein-
637 binding controls, respectively. The experiments were performed in triplicates for each
638 condition.

639

640 **Gene expression analysis**

641 Real-time PCR (RT-qPCR) was performed on cDNA from thyroid organoids from at least
642 three independent experiments. Total RNA was extracted from thyroid organoids by the
643 addition of lysis RLT Lysis buffer (Qiagen) + 1% 2-mercaptoethanol directly on the MTG
644 drop containing the organoids. For longer cultures (21 days), organoids were initially
645 incubated with a collagenase IV/Dispase II solution (described above) for 30-45 min.
646 Enzymes were inactivated by the addition of differentiation medium, cells were
647 centrifuged (500 g for 3 min), washed with PBS, and resuspended in RLT buffer. RNA
648 was isolated using the RNeasy micro kit (Qiagen) according to the manufacturer's

649 instructions. cDNA was generated by reverse transcription using the Superscript II kit
650 (Invitrogen). qPCR was performed in triplicates on cDNA (1:10 dilution) using Takyon™
651 No ROX SYBR 2X MasterMix blue dTTP (Eurogentec) and CFX Connect Real-Time
652 System (Biorad). Results are presented as linearized values normalized to the
653 housekeeping gene, β 2-microglobulin and the indicated reference value (2-DDCt). cAMP
654 condition was used as the control for all the comparisons. Primer sequences are described
655 in Supplementary Table 2.

656 **Bulk RNA sequencing and analysis**

657 Bulk RNA-seq was performed on day 31, using the cAMP, cAMP+4OHT (5 days) and
658 cAMP+4OHT+PD+LY (3 days) conditions (see protocol, Fig. 5A). RNA extraction was
659 performed as previously described (section “*Gene expression analysis*”), and
660 experiments were performed in duplicates. At least three distinct wells were pooled
661 together for each condition. RNA quality and concentration were evaluated using
662 Bioanalyser 2100 (Agilent) and RNA 6000 Nano Kit (Agilent). RNA integrity was
663 preserved, and no genomic DNA contamination was detected. Indexed cDNA libraries
664 were obtained using the TruSeq Stranded mRNA Sample Prep kit (Illumina) using an S2
665 flow cell, and sequences were produced using a 200 cycles reagent kit. The resulting high-
666 quality indexed cDNA libraries were quantified with the Quant-iT PicoGreen kit (Life
667 Sciences) and Infinite F200 Proplate reader (Tecan); DNA fragment size distribution was
668 examined with the 2100 Bioanalyzer (Agilent) using the DNA 1000 kit (Agilent).
669 Multiplexed libraries (10 μ M) were loaded onto flow cells and sequenced on the HiSeq
670 1500 system (Illumina) in high-output mode using the HiSeq Cluster Kit v4 (Illumina).
671 The sequenced data were uploaded on the galaxy web platform version 22.05.1, and the
672 public server, Data independent acquisition proteomics workbench (RRID:SCR_021862,
673 <https://usegalaxy.eu>), was used for mapping and counting analysis. Approximately 10

674 million paired-end reads were obtained per sample. After the removal of low-quality
675 bases and Illumina adapter sequences using Trimmomatic software¹⁰⁵
676 (RRID:SCR_011848), paired-end reads were mapped against the mouse reference
677 genome mm10 (GRCm38) using HISAT2 software¹⁰⁶, allowing soft clipping. Raw read
678 counts were obtained using HTseq count software with unstranded option¹⁰⁷. Low-
679 expressed genes were filtered using the EdgeR package in R Project for Statistical
680 Computing (<https://www.r-project.org>). Then, differential expression analysis was
681 performed using DESeq2 package¹⁰⁸. Fold change and adjusted p-value thresholds of 2
682 and 0.05, respectively were used to select differentially expressed genes (DEG). Gene
683 ontology and pathways enrichment analysis in up and down differentially expressed gene
684 lists was realized using EnrichR (<https://maayanlab.cloud/Enrichr/>). Transformed counts
685 corresponding to log2 (normalized counts +4) using the DESeq2 package were used for
686 further analysis and heatmap visualization. Thyroid differentiation score (TDS),
687 Enhanced Thyroid differentiation score (eTDS) and ERK activation score were calculated
688 as previously described⁶⁷. The list of the genes used for the score's calculation is provided
689 in Supplementary Table 3.

690

691 **Data availability**

692 Bulk RNA-seq data have been deposited in the NCBI Gene Expression Omnibus (GEO;
693 RRID:SCR_005012) under accession number GSE228281.

694

695 **Statistical analysis**

696 All statistical analysis were performed using GraphPad Prism 9. Comparison between
697 two groups and its statistical significance was tested using the nonparametric Mann-
698 Whitney U test. In contrast, comparisons between multiple groups was performed using

699 the nonparametric Kruskal-Wallis test. Data are displayed as median (IQR). Differences
700 were considered significant at $p < 0.05$ and presented as follows: * $p < 0.05$, ** $p < 0.01$,
701 *** $p < 0.001$, **** $p < 0.0001$. All the data presented are from at least three independent
702 experiments.

703 **Acknowledgements and Funding**

704 The authors acknowledge the ULB flow cytometry platform (C. Dubois), the ULB
705 genomic core facility (F. Libert and A. Lefort), LiMIF platform for confocal microscopy
706 (J.-M. Vanderwinden) and Eduardo Andrés Rios Morris for the contribution with the
707 imaging. We acknowledge the funding agencies that supported this study. The Belgian
708 National Fund for Scientific Research (FNRS) (PDR T.0140.14; PDR T.0230.18, CDR
709 J.0068.22, Televie 7.4633.17/7.4526.19) and the Fonds d'Encouragement à la Recherche
710 de l'Université Libre de Bruxelles (FER-ULB). The Belgian Fondation contre le cancer
711 (F/2020/1402; V.D.). FNRS (Chargé de Recherche, No.825745; M.R.). The cooperation
712 program CAPES-WBI (S.C. and A.L.M.). The Brazilian National Council for Scientific
713 and Technological Development (CNPq; M.R. and A.L.M), the Coordination for the
714 Improvement of Higher Education Personnel (CAPES; M.R. and A.L.M), the Brazilian
715 Society of Endocrinology and Metabolism (SBEM; M.R. and A.L.M) and the Fundação
716 de Amparo à Pesquisa do Estado do Rio Grande do Sul (FAPERGS; A.L.M). S.C is
717 Research Director at FNRS. M.R is researcher at ULB.

718

719 **Author contributions**

720 H.L., S.C. and M.R. developed the project, designed the experiments and analyzed the
721 data. L.H., T.P., S.G. and J.H. generated the plasmids and the G4 Rosaluc mESC line.
722 M.R. and A.S. generated the G4 RosaLuc TRE-Nkx2-1-Pax8_bTg-NES-Braf^{V637E}-ERT²
723 and TRE-Nkx2-1-Pax8_bTg-eGFP cell lines. H.L., M.R., B.F.F., A.S., O.M., L.C.,

724 M.K.P. B.A., L.C., performed the *in vitro* experiments and protocol set up. M.R. and P.G.
725 obtained confocal images. H.L., M.R. and A.T. performed bulk RNA-Sequencing and
726 analyzed the results. H.L. and A.T. performed the bioinformatics analysis. H.L. and M.R.
727 wrote the first draft and, A.L.M. and S.C. edited the manuscript. S.C., M.R. and A.L.M.
728 acquired funding for the project. All authors contributed to the article and approved the
729 submitted version.

730

731 **Competing interests**

732 All authors declare no competing interests.

733

734 **Correspondence** and requests for materials should be addressed to Mírian Romitti.

735

736 **REFERENCES**

- 737 1 Schutgens F, Clevers H. Human Organoids: Tools for Understanding Biology
738 and Treating Diseases. *Annual Review of Pathology: Mechanisms of Disease*
739 2020; **15**: 211–234.
- 740 2 Clevers H. Modeling Development and Disease with Organoids. *Cell* 2016; **165**:
741 1586–1597.
- 742 3 Kim J, Koo BK, Knoblich JA. Human organoids: model systems for human
743 biology and medicine. *Nat Rev Mol Cell Biol.* 2020; **21**: 571–584.
- 744 4 Antonica F, Kasprzyk DF, Opitz R, Iacovino M, Liao XH, Dumitrescu AM *et al.*
745 Generation of functional thyroid from embryonic stem cells. *Nature* 2012; **491**:
746 66–71.
- 747 5 Romitti M, Tourneur A, de Faria da Fonseca B, Doumont G, Gillotay P, Liao X-
748 H *et al.* Transplantable human thyroid organoids generated from embryonic stem
749 cells to rescue hypothyroidism. *Nat Commun* 2022; **13**: 7057.
- 750 6 Longmire TA, Ikonomou L, Hawkins F, Christodoulou C, Cao Y, Jean JC *et al.*
751 Efficient derivation of purified lung and thyroid progenitors from embryonic
752 stem cells. *Cell Stem Cell* 2012; **10**: 398–411.
- 753 7 Ma R, Latif R, Davies TF. Human embryonic stem cells form functional thyroid
754 follicles. *Thyroid* 2015; **25**: 455–461.
- 755 8 Ma R, Latif R, Davies TF. Thyroid follicle formation and thyroglobulin
756 expression in multipotent endodermal stem cells. *Thyroid* 2013; **23**: 385–391.
- 757 9 Ma R, Morshed SA, Latif R, Davies TF. TAZ Induction Directs Differentiation
758 of Thyroid Follicular Cells from Human Embryonic Stem Cells. *Thyroid* 2017;
759 **27**: 292–299.

760 10 Ma R, Shi R, Morshed SA, Latif R, Davies TF. Derivation and 97% Purification
761 of Human Thyroid Cells From Dermal Fibroblasts. *Front Endocrinol (Lausanne)*
762 2020; **11**: 446.

763 11 Kurmann AA, Serra M, Hawkins F, Rankin SA, Mori M, Astapova I *et al.*
764 Regeneration of Thyroid Function by Transplantation of Differentiated
765 Pluripotent Stem Cells. *Cell Stem Cell* 2015; **17**: 527–542.

766 12 Serra M, Alyssandratos KD, Hawkins F, McCauley KB, Jacob A, Choi J *et al.*
767 Pluripotent stem cell differentiation reveals distinct developmental pathways
768 regulating Lung-Versus Thyroid-Lineage specification. *Development*
769 (Cambridge) 2017; **144**: 3879–3893.

770 13 Dame K, Cincotta S, Lang AH, Sanghrajka RM, Zhang L, Choi J *et al.* Thyroid
771 Progenitors Are Robustly Derived from Embryonic Stem Cells through
772 Transient, Developmental Stage-Specific Overexpression of Nkx2-1. *Stem Cell*
773 *Reports* 2017; **8**: 216–225.

774 14 Ogundipe VML, Groen AH, Hosper N, Nagle PWK, Hess J, Faber H *et al.* Generation and Differentiation of Adult Tissue-Derived Human Thyroid
775 Organoids. *Stem Cell Reports* 2021; **16**: 913–925.

776 15 Liang J, Qian J, Yang L, Chen X, Wang X, Lin X *et al.* Modeling Human
777 Thyroid Development by Fetal Tissue-Derived Organoid Culture. *Advanced*
778 *Science* 2022; **9**. doi:10.1002/advs.202105568.

780 16 van der Vaart J, Bosmans L, Sijbesma SF, Knoops K, van de Wetering WJ, Otten
781 HG *et al.* Adult mouse and human organoids derived from thyroid follicular cells
782 and modeling of Graves' hyperthyroidism. *Proceedings of the National Academy*
783 *of Sciences* 2021; **118**. doi:10.1073/pnas.2117017118.

784 17 Boj SF, Hwang C-I, Baker LA, Chio IIC, Engle DD, Corbo V *et al.* Organoid
785 Models of Human and Mouse Ductal Pancreatic Cancer. *Cell* 2015; **160**: 324–
786 338.

787 18 Gao D, Vela I, Sboner A, Iaquinta PJ, Karthaus WR, Gopalan A *et al.* Organoid
788 Cultures Derived from Patients with Advanced Prostate Cancer. *Cell* 2014; **159**:
789 176–187.

790 19 Sato T, Stange DE, Ferrante M, Vries RGJ, van Es JH, van den Brink S *et al.*
791 Long-term Expansion of Epithelial Organoids From Human Colon, Adenoma,
792 Adenocarcinoma, and Barrett's Epithelium. *Gastroenterology* 2011; **141**: 1762–
793 1772.

794 20 van de Wetering M, Francies HE, Francis JM, Bounova G, Iorio F, Pronk A *et al.*
795 Prospective Derivation of a Living Organoid Biobank of Colorectal Cancer
796 Patients. *Cell* 2015; **161**: 933–945.

797 21 Drost J, Clevers H. Organoids in cancer research. *Nat Rev Cancer* 2018; **18**: 407–
798 418.

799 22 Gleave AM, Ci X, Lin D, Wang Y. A synopsis of prostate organoid
800 methodologies, applications, and limitations. *Prostate* 2020; **80**: 518–526.

801 23 Maenhoudt N, Vankelecom H. Protocol for establishing organoids from human
802 ovarian cancer biopsies. *STAR Protoc* 2021; **2**: 100429.

803 24 Gunti S, Hoke ATK, Vu KP, London NR. Organoid and Spheroid Tumor
804 Models: Techniques and Applications. *Cancers (Basel)* 2021; **13**: 874.

805 25 Saito Y, Onishi N, Takami H, Seishima R, Inoue H, Hirata Y *et al.* Development
806 of a functional thyroid model based on an organoid culture system. *Biochem*
807 *Biophys Res Commun* 2018; **497**: 783–789.

808 26 Chen D, Su X, Zhu L, Jia H, Han B, Chen H *et al.* Papillary thyroid cancer
809 organoids harboring BRAFV600E mutation reveal potentially beneficial effects
810 of BRAF inhibitor-based combination therapies. *J Transl Med* 2023; **21**: 9.
811 27 Vlachogiannis G, Hedayat S, Vatsiou A, Jamin Y, Fernández-Mateos J, Khan K
812 *et al.* Patient-derived organoids model treatment response of metastatic
813 gastrointestinal cancers. *Science (1979)* 2018; **359**: 920–926.
814 28 Drost J, van Jaarsveld RH, Ponsioen B, Zimberlin C, van Boxtel R, Buijs A *et al.*
815 Sequential cancer mutations in cultured human intestinal stem cells. *Nature*
816 2015; **521**: 43–47.
817 29 Matano M, Date S, Shimokawa M, Takano A, Fujii M, Ohta Y *et al.* Modeling
818 colorectal cancer using CRISPR-Cas9–mediated engineering of human intestinal
819 organoids. *Nat Med* 2015; **21**: 256–262.
820 30 Miura A, Yamada D, Nakamura M, Tomida S, Shimizu D, Jiang Y *et al.*
821 Oncogenic potential of human pluripotent stem cell-derived lung organoids with
822 <scp>HER2</scp> overexpression. *Int J Cancer* 2021; **149**: 1593–1604.
823 31 Nadauld LD, Garcia S, Natsoulis G, Bell JM, Miotke L, Hopmans ES *et al.*
824 Metastatic tumor evolution and organoid modeling implicate TGFBR2as a cancer
825 driver in diffuse gastric cancer. *Genome Biol* 2014; **15**: 428.
826 32 Li X, Nadauld L, Ootani A, Corney DC, Pai RK, Gevaert O *et al.* Oncogenic
827 transformation of diverse gastrointestinal tissues in primary organoid culture. *Nat
828 Med* 2014; **20**: 769–777.
829 33 Huang L, Holtzinger A, Jagan I, BeGora M, Lohse I, Ngai N *et al.* Ductal
830 pancreatic cancer modeling and drug screening using human pluripotent stem
831 cell– and patient-derived tumor organoids. *Nat Med* 2015; **21**: 1364–1371.
832 34 Lo Y-H, Karlsson K, Kuo CJ. Applications of organoids for cancer biology and
833 precision medicine. *Nat Cancer* 2020; **1**: 761–773.
834 35 Lim H, Devesa SS, Sosa JA, Check D, Kitahara CM. Trends in Thyroid Cancer
835 Incidence and Mortality in the United States, 1974–2013. *JAMA* 2017; **317**: 1338.
836 36 ROMITTI M, CEOLIN L, SIQUEIRA DR, FERREIRA CV, WAJNER SM,
837 MAIA AL. Signaling pathways in follicular cell-derived thyroid carcinomas. *Int
838 J Oncol* 2013; **42**: 19–28.
839 37 Kimura ET, Nikiforova MN, Zhu Z, Knauf JA, Nikiforov YE, Fagin JA. High
840 prevalence of BRAF mutations in thyroid cancer: genetic evidence for
841 constitutive activation of the RET/PTC-RAS-BRAF signaling pathway in
842 papillary thyroid carcinoma. *Cancer Res* 2003; **63**: 1454–7.
843 38 Fagin JA, Mitsiades N. Molecular pathology of thyroid cancer: diagnostic and
844 clinical implications. *Best Pract Res Clin Endocrinol Metab* 2008; **22**: 955–969.
845 39 Scheffel RS, Cristo AP de, Romitti M, Vargas CVF, Ceolin L, Zanella AB *et al.*
846 The BRAFV600E mutation analysis and risk stratification in papillary thyroid
847 carcinoma. *Arch Endocrinol Metab* 2020. doi:10.20945/2359-3997000000285.
848 40 Xing M. The T1799A BRAF mutation is not a germline mutation in familial
849 nonmedullary thyroid cancer. *Clin Endocrinol (Oxf)* 2005; **63**: 263–266.
850 41 Chakravarty D, Santos E, Ryder M, Knauf JA, Liao X-H, West BL *et al.* Small-
851 molecule MAPK inhibitors restore radioiodine incorporation in mouse thyroid
852 cancers with conditional BRAF activation. *Journal of Clinical Investigation*
853 2011; **121**: 4700–4711.
854 42 Zaman, Wu, Bivona. Targeting Oncogenic BRAF: Past, Present, and Future.
855 *Cancers (Basel)* 2019; **11**: 1197.

856 43 Agrawal N, Akbani R, Aksoy BA, Ally A, Arachchi H, Asa SL *et al.* Integrated
857 Genomic Characterization of Papillary Thyroid Carcinoma. *Cell* 2014; **159**: 676–
858 690.

859 44 Romei C, Fugazzola L, Puxeddu E, Frasca F, Viola D, Muzza M *et al.*
860 Modifications in the Papillary Thyroid Cancer Gene Profile Over the Last 15
861 Years. *J Clin Endocrinol Metab* 2012; **97**: E1758–E1765.

862 45 Sabra MM, Dominguez JM, Grewal RK, Larson SM, Ghossein RA, Tuttle RM *et*
863 *al.* Clinical Outcomes and Molecular Profile of Differentiated Thyroid Cancers
864 With Radioiodine-Avid Distant Metastases. *J Clin Endocrinol Metab* 2013; **98**:
865 E829–E836.

866 46 Xing M. BRAFV600E Mutation and Papillary Thyroid Cancer. *JAMA* 2013; **310**:
867 535.

868 47 Scheffel RS, Cristo AP de, Romitti M, Vargas CVF, Ceolin L, Zanella AB *et al.*
869 The BRAFV600E mutation analysis and risk stratification in papillary thyroid
870 carcinoma. *Arch Endocrinol Metab* 2021. doi:10.20945/2359-3997000000285.

871 48 Liu R, Bishop J, Zhu G, Zhang T, Ladenson PW, Xing M. Mortality Risk
872 Stratification by Combining BRAF V600E and TERT Promoter Mutations in
873 Papillary Thyroid Cancer. *JAMA Oncol* 2017; **3**: 202.

874 49 Boucail L, Seshan V, Williams M, Knauf JA, Saqcena M, Ghossein RA *et al.*
875 Characterization of Subtypes of BRAF-Mutant Papillary Thyroid Cancer Defined
876 by Their Thyroid Differentiation Score. *J Clin Endocrinol Metab* 2022; **107**:
877 1030–1039.

878 50 Chen D, Tan Y, Li Z, Li W, Yu L, Chen W *et al.* Organoid Cultures Derived
879 From Patients With Papillary Thyroid Cancer. *J Clin Endocrinol Metab* 2021;
880 **106**: 1410–1426.

881 51 Sondorp LHJ, Ogundipe VML, Groen AH, Kelder W, Kemper A, Links TP *et al.*
882 Patient-Derived Papillary Thyroid Cancer Organoids for Radioactive Iodine
883 Refractory Screening. *Cancers (Basel)* 2020; **12**: 3212.

884 52 Pecce V, Sponziello M, Bini S, Grani G, Durante C, Verrienti A. Establishment
885 and maintenance of thyroid organoids from human cancer cells. *STAR Protoc*
886 2022; **3**: 101393.

887 53 Chen D, Su X, Zhu L, Jia H, Han B, Chen H *et al.* Papillary thyroid cancer
888 organoids harboring BRAFV600E mutation reveal potentially beneficial effects
889 of BRAF inhibitor-based combination therapies. *J Transl Med* 2023; **21**: 9.

890 54 Yang H, Liang Q, Zhang J, Liu J, Wei H, Chen H *et al.* Establishment of
891 papillary thyroid cancer organoid lines from clinical specimens. *Front
892 Endocrinol (Lausanne)* 2023; **14**. doi:10.3389/fendo.2023.1140888.

893 55 Veschi V, Turdo A, Modica C, Verona F, Di Franco S, Gaggianesi M *et al.*
894 Recapitulating thyroid cancer histotypes through engineering embryonic stem
895 cells. *Nat Commun* 2023; **14**: 1351.

896 56 Ortiz O, Wurst W, Kühn R. Reversible and tissue-specific activation of MAP
897 kinase signaling by tamoxifen in *braf*^{V637} ER^{T2} mice. *genesis* 2013; **51**: 448–
898 455.

899 57 Antonica F, Kasprzyk DF, Schiavo AA, Romitti M, Costagliola S. Generation of
900 Functional Thyroid Tissue Using 3D-Based Culture of Embryonic Stem Cells.
901 2017, pp 85–95.

902 58 Romitti M, Eski SE, Fonseca BF, Gillotay P, Singh SP, Costagliola S. Single-
903 Cell Trajectory Inference Guided Enhancement of Thyroid Maturation In Vitro
904 Using TGF-Beta Inhibition. *Front Endocrinol (Lausanne)* 2021; **12**.
905 doi:10.3389/fendo.2021.657195.

906 59 Knauf JA, Ma X, Smith EP, Zhang L, Mitsutake N, Liao X-H *et al.* Targeted
907 Expression of BRAFV600E in Thyroid Cells of Transgenic Mice Results in
908 Papillary Thyroid Cancers that Undergo Dedifferentiation. *Cancer Res* 2005; **65**:
909 4238–4245.

910 60 Schoultz E, Liang S, Carlsson T, Filges S, Ståhlberg A, Fagman H *et al.* Tissue
911 specificity of oncogenic BRAF targeted to lung and thyroid through a shared
912 lineage factor. *iScience* 2023; **26**: 107071.

913 61 Tang W-W, Huang C, Tang C, Xu J, Wang H. Galectin-3 may serve as a
914 potential marker for diagnosis and prognosis in papillary thyroid carcinoma: a
915 meta-analysis. *Onco Targets Ther* 2016; : 455.

916 62 Xia S, Wang C, Postma EL, Yang Y, Ni X, Zhan W. Fibronectin 1 promotes
917 migration and invasion of papillary thyroid cancer and predicts papillary thyroid
918 cancer lymph node metastasis. *Onco Targets Ther* 2017; **Volume 10**: 1743–1755.

919 63 Sponziello M, Rosignolo F, Celano M, Maggisano V, Pecce V, De Rose RF *et al.*
920 Fibronectin-1 expression is increased in aggressive thyroid cancer and favors the
921 migration and invasion of cancer cells. *Mol Cell Endocrinol* 2016; **431**: 123–132.

922 64 Reischmann N, Andrieux G, Griffin R, Reinheckel T, Boerries M, Brummer T.
923 BRAFV600E drives dedifferentiation in small intestinal and colonic organoids
924 and cooperates with mutant p53 and Apc loss in transformation. *Oncogene* 2020;
925 **39**: 6053–6070.

926 65 Chandeck C, Mooi WJ. Oncogene-induced Cellular Senescence. *Adv Anat Pathol*
927 2010; **17**: 42–48.

928 66 Bellelli R, Vitagliano D, Federico G, Marotta P, Tamburrino A, Salerno P *et al.*
929 Oncogene-induced senescence and its evasion in a mouse model of thyroid
930 neoplasia. *Mol Cell Endocrinol* 2018; **460**: 24–35.

931 67 Dunn LA, Sherman EJ, Baxi SS, Tchekmedyan V, Grewal RK, Larson SM *et al.*
932 Vemurafenib Redifferentiation of BRAF Mutant, RAI-Refactory Thyroid
933 Cancers. *J Clin Endocrinol Metab* 2019; **104**: 1417–1428.

934 68 Kogai T, Brent GA. The sodium iodide symporter (NIS): Regulation and
935 approaches to targeting for cancer therapeutics. *Pharmacol Ther* 2012; **135**: 355–
936 370.

937 69 Azouzi N, Cailloux J, Cazarin JM, Knauf JA, Cracchiolo J, Al Ghuzlan A *et al.*
938 NADPH Oxidase NOX4 Is a Critical Mediator of BRAF^{V600E}-Induced
939 Downregulation of the Sodium/Iodide Symporter in Papillary Thyroid
940 Carcinomas. *Antioxid Redox Signal* 2017; **26**: 864–877.

941 70 Subbiah V, Kreitman RJ, Wainberg ZA, Cho JY, Schellens JHM, Soria JC *et al.*
942 Dabrafenib plus trametinib in patients with BRAF V600E-mutant anaplastic
943 thyroid cancer: updated analysis from the phase II ROAR basket study. *Annals of*
944 *Oncology* 2022; **33**: 406–415.

945 71 Leboulleux S, Do Cao C, Zerdoud S, Attard M, Bournaud C, Lacroix L *et al.* A
946 Phase II Redifferentiation Trial with Dabrafenib-Trametinib and 131I in
947 Metastatic Radioactive Iodine Refractory BRAF p.V600E-Mutated Differentiated
948 Thyroid Cancer. *Clinical Cancer Research* 2023; **29**: 2401–2409.

949 72 Califano I, Smulever A, Jerkovich F, Pitoia F. Advances in the management of
950 anaplastic thyroid carcinoma: transforming a life-threatening condition into a
951 potentially treatable disease. *Rev Endocr Metab Disord* 2023.
952 doi:10.1007/s11154-023-09833-1.

953 73 Saqcena M, Leandro-Garcia LJ, Maag JLV, Tchekmedyan V, Krishnamoorthy
954 GP, Tamarapu PP *et al.* SWI/SNF Complex Mutations Promote Thyroid Tumor

955 956 Progression and Insensitivity to Redifferentiation Therapies. *Cancer Discov*
2021; **11**: 1158–1175.

957 74 Qiu W, Yang Z, Fan Y, Zheng Q. ZNRF3 is downregulated in papillary thyroid
958 carcinoma and suppresses the proliferation and invasion of papillary thyroid
959 cancer cells. *Tumor Biology* 2016; **37**: 12665–12672.

960 75 Han J, Chen M, Wang Y, Gong B, Zhuang T, Liang L *et al.* Identification of
961 Biomarkers Based on Differentially Expressed Genes in Papillary Thyroid
962 Carcinoma. *Sci Rep* 2018; **8**: 9912.

963 76 Yoo S-K, Song YS, Lee EK, Hwang J, Kim HH, Jung G *et al.* Integrative
964 analysis of genomic and transcriptomic characteristics associated with
965 progression of aggressive thyroid cancer. *Nat Commun* 2019; **10**: 2764.

966 77 Davies H, Bignell GR, Cox C, Stephens P, Edkins S, Clegg S *et al.* Mutations of
967 the BRAF gene in human cancer. *Nature* 2002; **417**: 949–954.

968 78 Dhomen N, Marais R. New insight into BRAF mutations in cancer. *Curr Opin
969 Genet Dev* 2007; **17**: 31–39.

970 79 Nikiforov YE, Nikiforova MN. Molecular genetics and diagnosis of thyroid
971 cancer. *Nat Rev Endocrinol* 2011; **7**: 569–580.

972 80 Cheng L, Lopez-Beltran A, Massari F, MacLennan GT, Montironi R. Molecular
973 testing for BRAF mutations to inform melanoma treatment decisions: a move
974 toward precision medicine. *Modern Pathology* 2018; **31**: 24–38.

975 81 Schirripa M, Biason P, Lonardi S, Pella N, Pino MS, Urbano F *et al.* Class 1, 2,
976 and 3 BRAF-Mutated Metastatic Colorectal Cancer: A Detailed Clinical,
977 Pathologic, and Molecular Characterization. *Clinical Cancer Research* 2019; **25**:
978 3954–3961.

979 82 Pisapia P, Pepe F, Malapelle U, Troncone G. Mutations in Lung Cancer. *Acta
980 Cytol* 2019; **63**: 247–250.

981 83 Pisapia P, Pepe F, Iaccarino A, Sgariglia R, Nacchio M, Russo G *et al.* BRAF: A
982 Two-Faced Janus. *Cells* 2020; **9**: 2549.

983 84 Pavlick AC, Fecher L, Ascierto PA, Sullivan RJ. Frontline Therapy for BRAF-
984 Mutated Metastatic Melanoma: How Do You Choose, and Is There One Correct
985 Answer? *American Society of Clinical Oncology Educational Book* 2019; : 564–
986 571.

987 85 Anguera G, Majem M. BRAF inhibitors in metastatic non-small cell lung cancer.
988 *J Thorac Dis* 2018; **10**: 589–592.

989 86 Haugen BR, Alexander EK, Bible KC, Doherty GM, Mandel SJ, Nikiforov YE *et
990 al.* 2015 American Thyroid Association Management Guidelines for Adult
991 Patients with Thyroid Nodules and Differentiated Thyroid Cancer: The American
992 Thyroid Association Guidelines Task Force on Thyroid Nodules and
993 Differentiated Thyroid Cancer. *Thyroid* 2016; **26**: 1–133.

994 87 Schmidbauer B, Menhart K, Hellwig D, Grosse J. Differentiated Thyroid
995 Cancer—Treatment: State of the Art. *Int J Mol Sci* 2017; **18**: 1292.

996 88 Kim TY, Kim WG, Kim WB, Shong YK. Current Status and Future Perspectives
997 in Differentiated Thyroid Cancer. *Endocrinology and Metabolism* 2014; **29**: 217.

998 89 Ahn B-C. Personalized Medicine Based on Theranostic Radioiodine Molecular
999 Imaging for Differentiated Thyroid Cancer. *Biomed Res Int* 2016; **2016**: 1–9.

1000 90 Paeng JC, Kang KW, Park DJ, Oh SW, Chung J-K. Alternative Medical
1001 Treatment for Radioiodine-Refractory Thyroid Cancers. *Nucl Med Mol Imaging*
1002 2011; **45**: 241–247.

1003 91 Brose MS, Nutting CM, Jarzab B, Elisei R, Siena S, Bastholt L *et al.* Sorafenib in
1004 radioactive iodine-refractory, locally advanced or metastatic differentiated

1005 1006 thyroid cancer: a randomised, double-blind, phase 3 trial. *The Lancet* 2014; **384**:
319–328.

1007 92 Schlumberger M, Tahara M, Wirth LJ, Robinson B, Brose MS, Elisei R *et al.*
1008 Lenvatinib versus Placebo in Radioiodine-Refractory Thyroid Cancer. *New
England Journal of Medicine* 2015; **372**: 621–630.

1009 93 Ho AL, Grewal RK, Leboeuf R, Sherman EJ, Pfister DG, Deandreis D *et al.*
1010 Selumetinib-Enhanced Radioiodine Uptake in Advanced Thyroid Cancer. *New
England Journal of Medicine* 2013; **368**: 623–632.

1011 94 Rothenberg SM, Daniels GH, Wirth LJ. Redifferentiation of Iodine-Refractory
1012 BRAF V600E-Mutant Metastatic Papillary Thyroid Cancer with Dabrafenib—
1013 Response. *Clinical Cancer Research* 2015; **21**: 5640–5641.

1014 95 Buffet C, Wassermann J, Hecht F, Leenhardt L, Dupuy C, Groussin L *et al.*
1015 Redifferentiation of radioiodine-refractory thyroid cancers. *Endocr Relat Cancer*
1016 2020; **27**: R113–R132.

1017 96 Riesco-Eizaguirre G, Santisteban P. A perspective view of sodium iodide
1018 symporter research and its clinical implications. *Eur J Endocrinol* 2006; **155**:
495–512.

1019 97 Czarnecka AM, Bartnik E, Fiedorowicz M, Rutkowski P. Targeted Therapy in
1020 Melanoma and Mechanisms of Resistance. *Int J Mol Sci* 2020; **21**: 4576.

1021 98 Flaherty KT, Infante JR, Daud A, Gonzalez R, Kefford RF, Sosman J *et al.*
1022 Combined BRAF and MEK Inhibition in Melanoma with BRAF V600
1023 Mutations. *New England Journal of Medicine* 2012; **367**: 1694–1703.

1024 99 Larkin J, Ascierto PA, Dréno B, Atkinson V, Liszkay G, Maio M *et al.*
1025 Combined Vemurafenib and Cobimetinib in BRAF-Mutated Melanoma. *New
1026 England Journal of Medicine* 2014; **371**: 1867–1876.

1027 100 Dummer R, Ascierto PA, Gogas HJ, Arance A, Mandala M, Liszkay G *et al.*
1028 Encorafenib plus binimatinib versus vemurafenib or encorafenib in patients with
1029 BRAF -mutant melanoma (COLUMBUS): a multicentre, open-label, randomised
1030 phase 3 trial. *Lancet Oncol* 2018; **19**: 603–615.

1031 101 Smalley KSM. Increased immunity and BRAF inhibition: Yet another argument
1032 for combination therapy? *Pharmacol Res* 2016; **113**: 719–720.

1033 102 Roskoski R. Targeting oncogenic Raf protein-serine/threonine kinases in human
1034 cancers. *Pharmacol Res* 2018; **135**: 239–258.

1035 103 Zhao X, Wang JR, Dadu R, Busaidy NL, Xu L, Learned KO *et al.* Surgery After
1036 BRAF-Directed Therapy Is Associated with Improved Survival in BRAF^{V600E}
1037 Mutant Anaplastic Thyroid Cancer: A Single-Center Retrospective Cohort Study.
1038 *Thyroid* 2023; **33**: 484–491.

1039 104 Haenebalcke L, Goossens S, Naessens M, Kruse N, Ghahremani MF, Bartunkova
1040 S *et al.* Efficient ROSA26-Based Conditional and/or Inducible Transgenesis
1041 Using RMCE-Compatible F1 Hybrid Mouse Embryonic Stem Cells. *Stem Cell
Rev Rep* 2013; **9**: 774–785.

1042 105 Bolger AM, Lohse M, Usadel B. Trimmomatic: a flexible trimmer for Illumina
1043 sequence data. *Bioinformatics* 2014; **30**. doi:10.1093/bioinformatics/btu170.

1044 106 Kim D, Langmead B, Salzberg SL. HISAT: a fast spliced aligner with low
1045 memory requirements. *Nat Methods* 2015; **12**. doi:10.1038/nmeth.3317.

1046 107 Hao Y, Hao S, Andersen-Nissen E, Mauck WM, Zheng S, Butler A *et al.*
1047 Integrated analysis of multimodal single-cell data. *Cell* 2021; **184**: 3573–
1048 3587.e29.

1049 108 Love MI, Huber W, Anders S. Moderated estimation of fold change and
1050 dispersion for RNA-seq data with DESeq2. *Genome Biol* 2014; **15**: 550.

1051 109
1052 110

1055

1056

1057

1058

1059 **FIGURE LEGENDS**

1060

1061 **Fig. 1 mESC_Nkx2-1/Pax8_bTg_Braf^{V637E} cell line differentiation into thyroid**
1062 **organoids.** Scheme of the thyroid differentiation protocol and Braf^{V637E} induction in
1063 mature thyroid follicles (A). Differentiation of mESC_Nkx2-1/Pax8_bTg_Braf^{V637E} cell
1064 line promotes expression of the main thyroid genes and Braf^{V637E} exogenous (B). Control
1065 corresponds to the - Dox condition. Immunofluorescence staining showing Nkx2-1 and
1066 Tg co-expressing cells organized in follicular structures (C), which are accumulating the
1067 thyroid hormone precursor, Tg-I, inside the lumen compartment (D). The follicular
1068 enrichment (FE) procedure significantly increased the expression levels of thyroid genes
1069 (E) while keeping the structural organization of the follicles evidenced by Nis basolateral
1070 localization (F) and its functionality, with Tg-I accumulation (G). Values represent the
1071 median (IQR) of 3 independent experiments with individual values shown (*p<0.05 ;
1072 **p<0.01 ; ***p<0.001; Mann-Whitney U test). Scale bars, 50 μ m and 10 μ m for high
1073 magnification follicles.

1074

1075 **Fig. 2 Effect of the Braf^{V637E} oncogene induction on mature thyroid follicles.**

1076 Schematic representation of thyroid differentiation, Braf^{V637E} oncogene expression on
1077 thyroid cells, and its activation under tamoxifen (4OHT) treatment (A). Western blot
1078 demonstrates an increase of phospho-ERK (pERK) 48 hours after the addition of 4OHT
1079 to the organoids culture (B). Beta-actin was used as a loading control for the immunoblot

1080 experiments. The image represents one experiment from 3 experimental replicates. Gene
1081 expression analysis showing the inhibitory effect of $\text{Braf}^{\text{V637E}}$ -oncogene activation on
1082 thyroid genes after 6 hours (C), 48 hours (D), 7 days (E) and 21 days (F) of 4OHT
1083 treatment. For each time point gene expression levels of the cAMP+4OHT treated cells
1084 were compared to the control (cAMP) levels. Bar graphs represent the median (IQR) of
1085 at least 3 independent experiments with individual values shown. (*p<0.05 ; **p<0.01 ;
1086 ***p<0.001; ****p<0.0001; Mann-Whitney U test). Proportions of proliferating
1087 (Nkx2.1/BrDU+) (G) and apoptotic (Nkx2.1/Caspase3+) (H) cells among control
1088 (cAMP) and $\text{Braf}^{\text{V637E}}$ -induced (4OHT) organoids after 7 and 21 days of 4OHT treatment.
1089 For the proliferation assay, isotype and -BrdU conditions were used as negative controls
1090 for flow cytometry gating. As a positive control for apoptosis, staurosporine treatment
1091 (24 h) was used to determine Caspase 3 expression. Bar graphs represent the median
1092 (IQR) of at least 3 independent experiments with individual values shown. cAMP was
1093 used as control for comparisons. (**p<0.01; Mann-Whitney U test).

1094

1095 **Fig. 3 Morphological changes on thyroid follicles caused by $\text{Braf}^{\text{V637E}}$ activation.**
1096 cAMP-treated thyroid cells show follicular organization with Nkx2-1 nuclear expression
1097 and Tg accumulation in the luminal compartment. In contrast, after 48 h of $\text{Braf}^{\text{V637E}}$
1098 oncogene induction by 4OHT, most of the cells are not organized into follicular structures
1099 and a great proportion is expressing very low levels of Tg (A). Higher magnification
1100 images showing the follicular organization of the thyroid cells in the control condition
1101 (48 h), with proper expression of Nkx2-1 and/or Tg (B), E-cadherin (C), Zo-1 (D), Nis
1102 (E) and Tg-I (F) accumulation in the lumen. While in the 4OHT condition the follicular
1103 organization is disrupted as well as its function. Nkx2-1 and Tg co-staining in control
1104 (cAMP) and $\text{Braf}^{\text{V637E}}$ -induced (4OHT) cells for 7 days (G) and 21 days (H) shows clear

1105 changes in thyroid morphology evidenced by the heterogeneity of Nkx2-1 cells which
1106 mostly do not express Tg or at low levels at day 7, while at day 21 a higher proportion of
1107 Nkx2-1 cells are Tg positive. Hoescht (shown in blue) was used for nuclei staining. Scale
1108 bars, 20 μ m (A), 10 μ m (B-F) and 50 μ m (G-H).

1109

1110 **Fig. 4 Drug screening reveals that VPA and MAPK/PI3K inhibition can restore Nis**
1111 **expression in Braf^{V637E}-induced cells.** Schematic representation of the protocol used for
1112 drug screening experiments (A). qPCR data show that 4OHT-treated organoids (4 days)
1113 treated with MEK (PD0325901; PD) and PI3K (LY294002; LY) inhibitors isolated
1114 increase but do not restore *Nis* expression to control (cAMP) levels. However, when
1115 combined, *Nis* expression reached cAMP levels. On the other hand, the HDAC inhibitor
1116 (VPA) can recover *Nis* expression (B) by itself. Bar graphs represent the median (IQR)
1117 of at least 4 independent experiments with individual values shown. Comparisons were
1118 performed against the cAMP condition. (**p<0.05 ; ***p<0.001 ; Mann-Whitney U test).
1119 Confocal images show downregulation of the Nis transporter in 4OHT condition, which
1120 is restored by VPA treatment. However, the expression pattern differs from the control
1121 (cAMP) condition. Co-inhibition of MAPK and PI3K pathways associated or not to VPA
1122 treatment restores Nis protein expression at the basolateral membrane of the properly
1123 organized follicles (C). Scale bars, 10 μ m. Gene expression analysis shows that
1124 PD0325901 and LY294002 co-treatment recover the *Tg* (D), *TSHR* (E), and *Tpo* (F)
1125 mRNA to cAMP levels. Bar graphs represent the median (IQR) of at least 3 independent
1126 experiments with individual values shown. Comparisons were performed against the
1127 cAMP condition. (*p<0.05 ; **p<0.01 ; ***p<0.001; ***p<0.0001; Mann-Whitney U
1128 test). Immunostaining for Nkx2-1 and Tg shows that proteins levels are similar to controls
1129 (cAMP) while follicular organization (G, H) and luminal Tg-I accumulation were

1130 restored under PD+LY and PD+LY+VPA conditions (I). Scale bars, 20 μ m (G), 50 μ m
1131 (H), and 10 μ m (I). Organification assay shows recovery of Iodine uptake (J), Protein-
1132 bound to 125I (K), and % of iodine Organification (L) in PD+LY and PD+LY+VPA
1133 conditions. Bar graphs represent the median (IQR) of at least 3 independent experiments
1134 with individual values shown. Comparisons were performed against the cAMP condition.
1135 (**p<0.01 ; ***p<0.0001; Mann-Whitney U test).

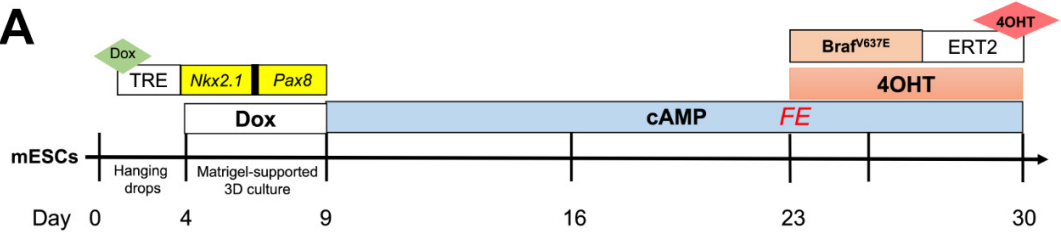
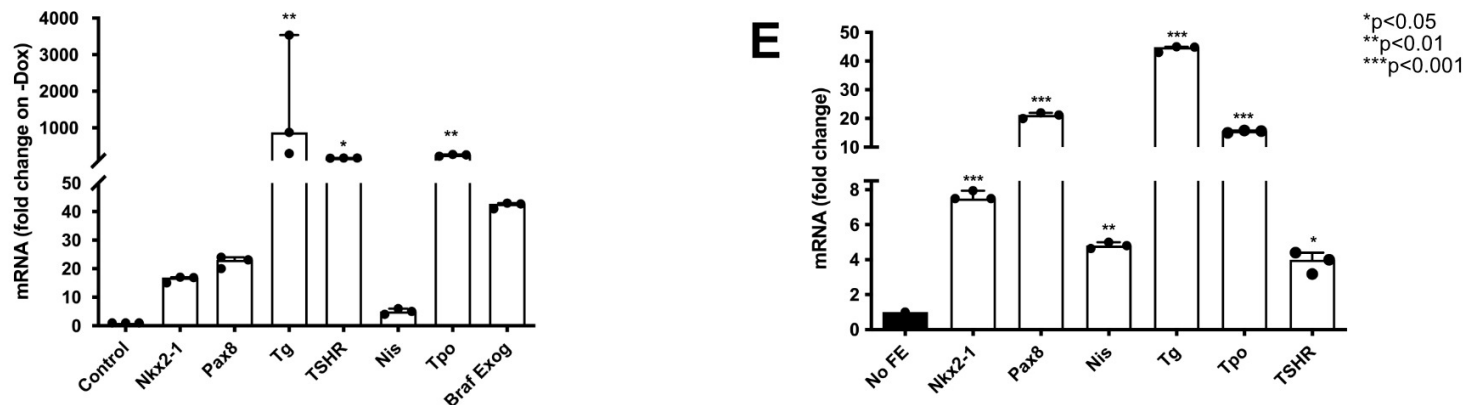
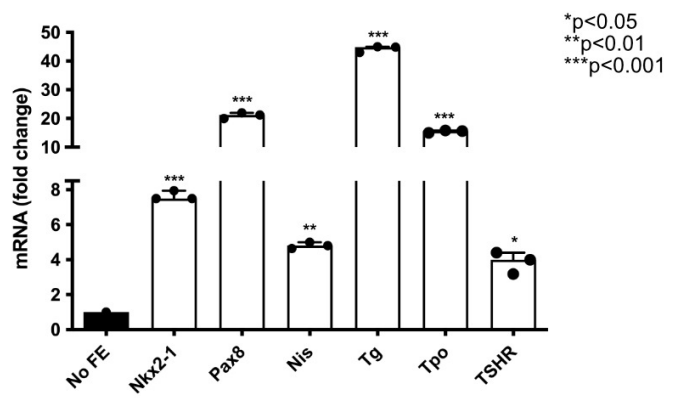
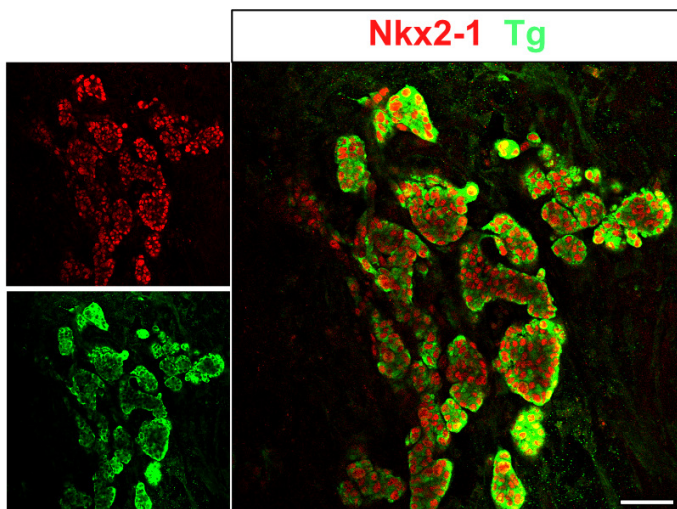
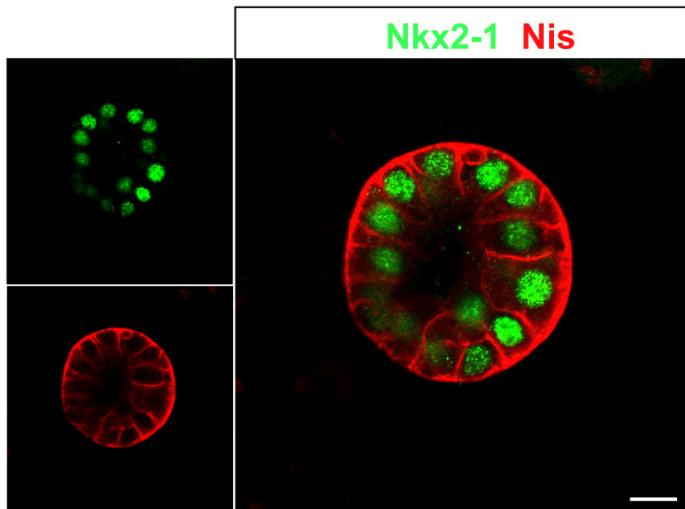
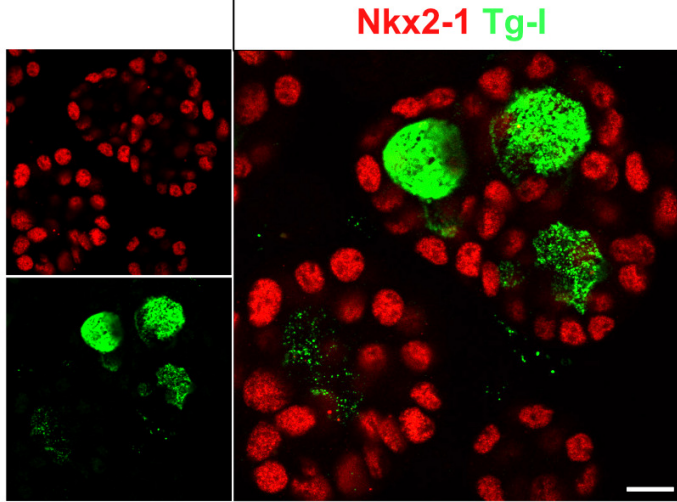
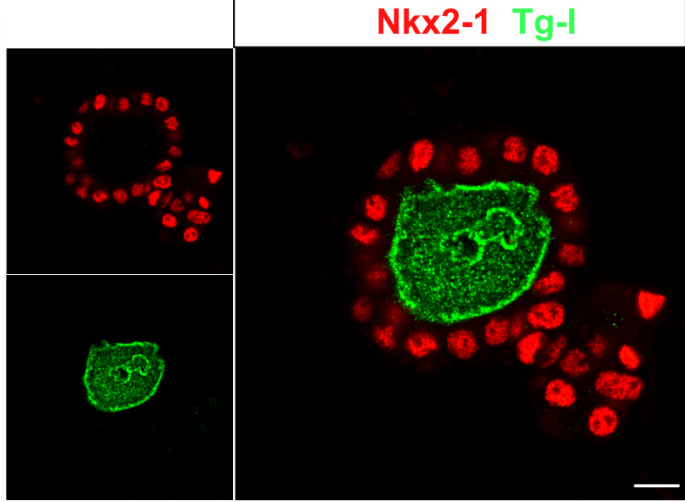
1136

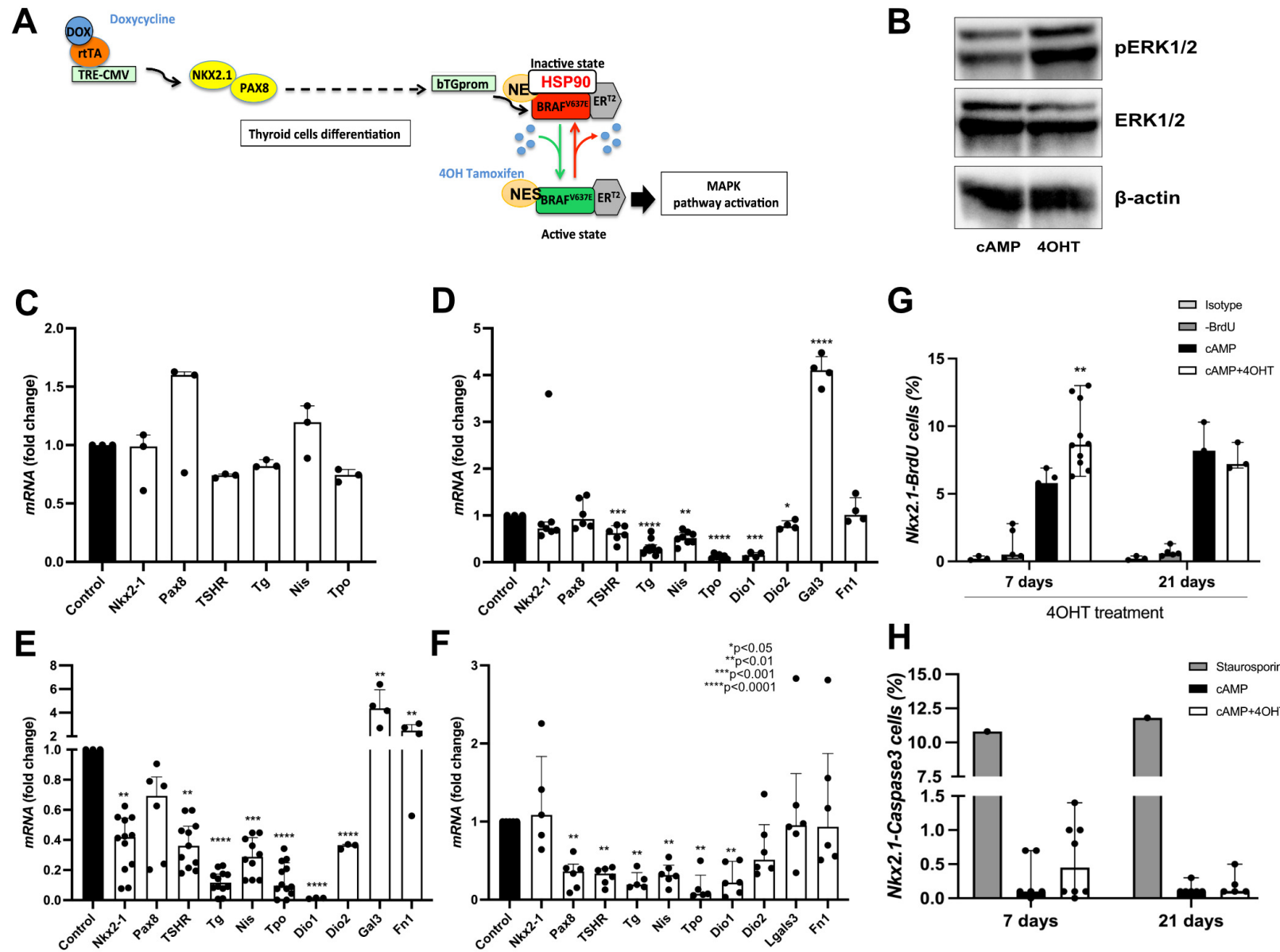
1137 **Fig. 5 Dabrafenib and trametinib effect on redifferentiation of Braf^{V637E}-expressing**
1138 **cells.** Braf^{V637E}-expressing organoids treated with Dabrafenib and Trametinib restore the
1139 expression of *Nis* to cAMP levels. However, a greater increase is observed under
1140 Trametinib+LY co-treatment (A). Recovery of *Tg* (B), *TSHR* (C) and *Tpo* (D) mRNA to
1141 control levels was observed under co-treatment of Dabrafenib and Trametinib with the
1142 PI3K inhibitor (LY). Bar graphs represent the median (IQR) of at least 4 independent
1143 experiments with individual values shown. Comparisons were performed against the
1144 cAMP condition. (*p<0.05 ; **p<0.01; Mann-Whitney U test). Confocal images show
1145 that Dabrafenib and Trametinib isolated or combined to PI3K inhibitor (LY) also induce
1146 *Tg* and *Nis* protein levels while restoring the follicular structure (in a proportion of cells)
1147 and *Tg*-I accumulation in the lumen (E). Hoescht (shown in blue) was used for nuclei
1148 staining. Scale bars, 20 μ m (*Tg* and *Tg*-I) and 10 μ m (*Nis*). Proportions of proliferating
1149 (*Nkx2.1/BrDU*+ (F) and apoptotic (*Nkx2.1/Caspase3*+ (G) cells among control
1150 (cAMP), Braf^{V637E}-induced (4OHT) and inhibitors (4OHT+inhibitors)-treated organoids
1151 after. For the proliferation assay, isotype and -BrdU conditions were used as negative
1152 controls for flow cytometry gating. As a positive control for apoptosis, staurosporine
1153 treatment (24 h) was used to determine Caspase 3 expression. Bar graphs represent the
1154 median (IQR) of at least 3 independent experiments with individual values shown.

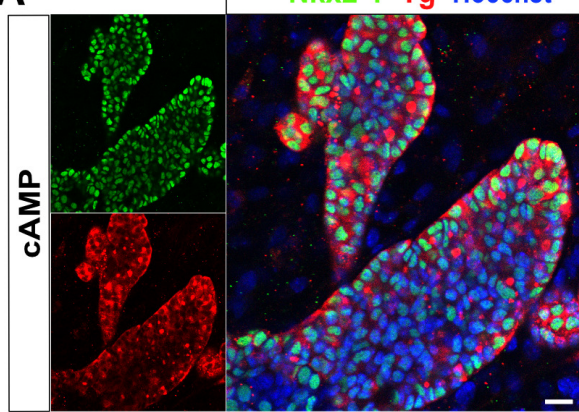
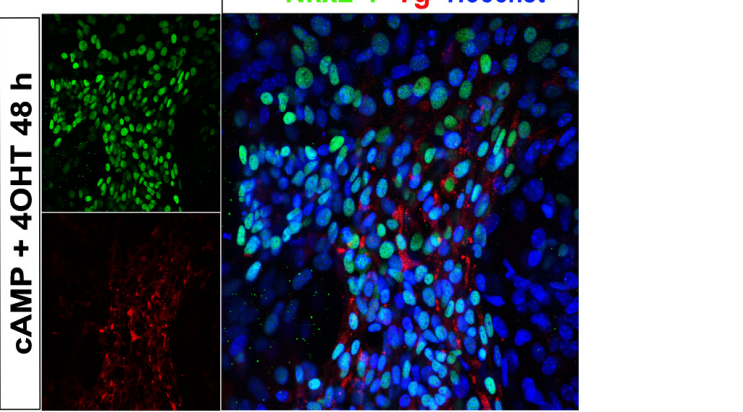
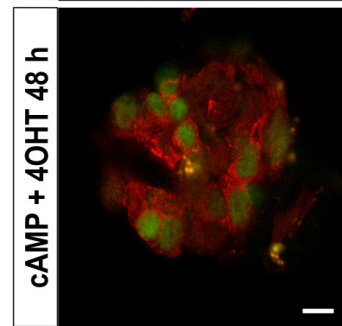
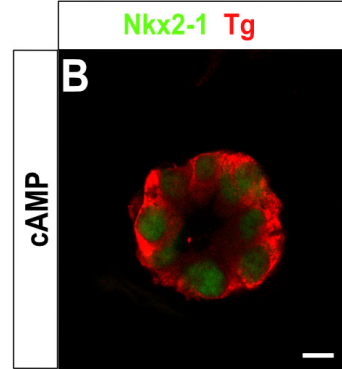
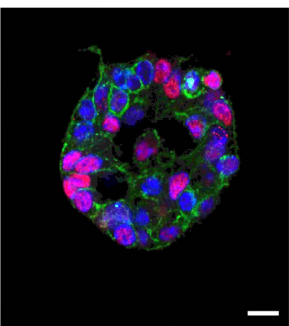
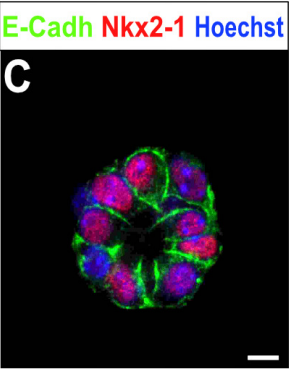
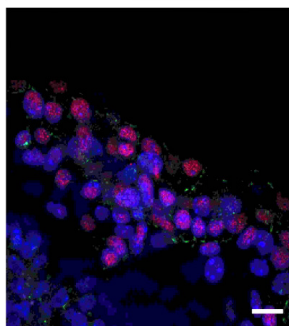
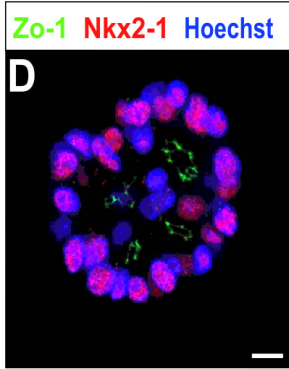
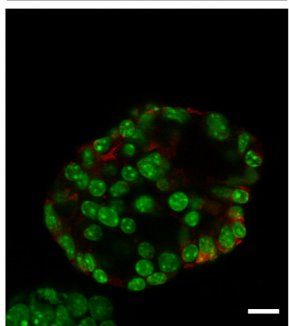
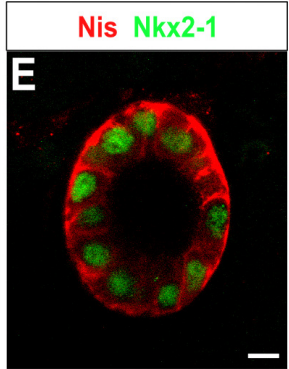
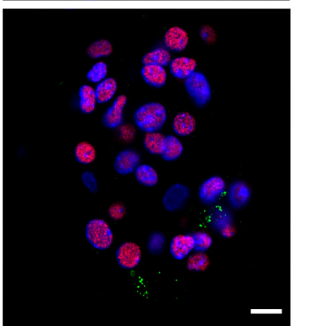
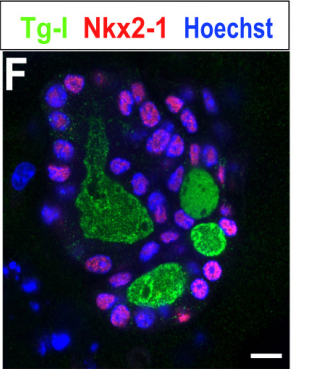
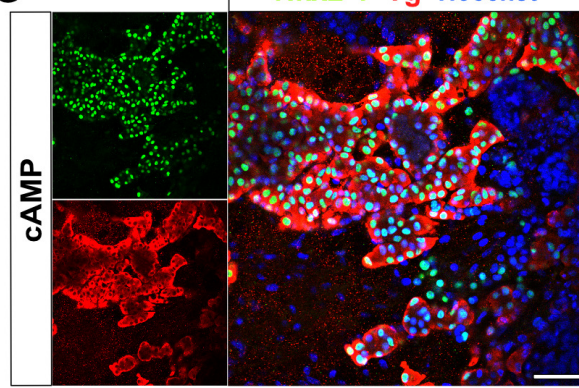
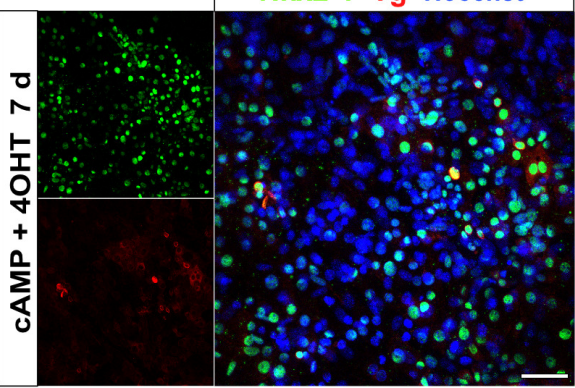
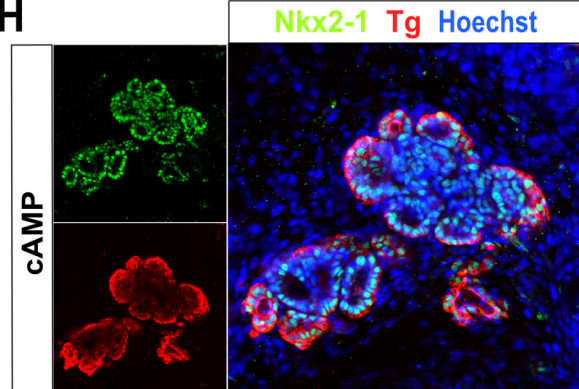
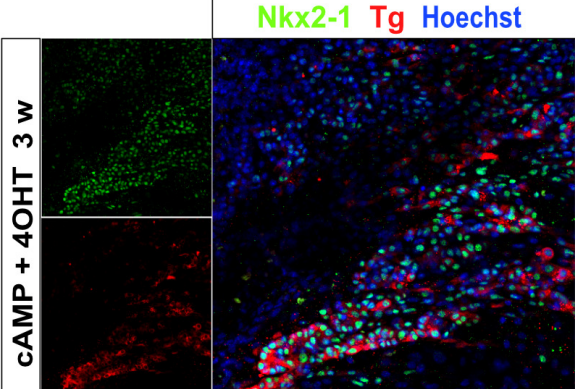
1155 Comparisons were performed against the 4OHT condition. (*p<0.05 ; **p<0.01 ; Mann-
1156 Whitney U test). Western blot shows an increase of phospho-ERK (pERK) 7 days after
1157 the addition of 4OHT to the organoids culture when compared to cAMP control.
1158 Conversely, the treatment with Trametinib+LY resulted in pERK reduction compared to
1159 the 4OHT condition. (B). Beta-actin was used as a loading control for the immunoblot
1160 experiments. The image represents one experiment from 3 experimental replicates.

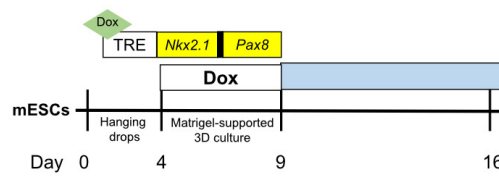
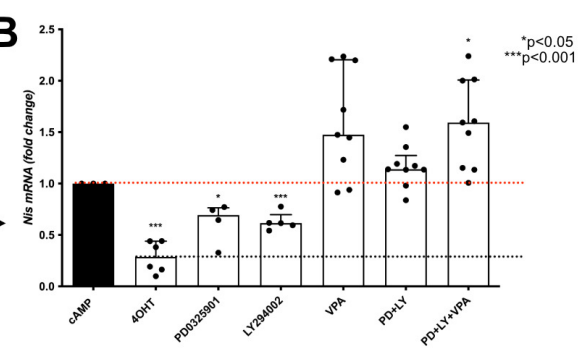
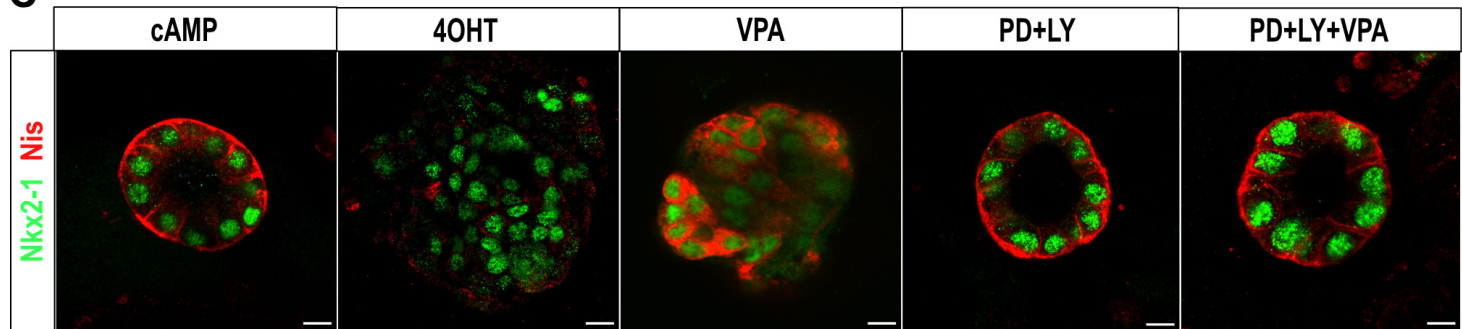
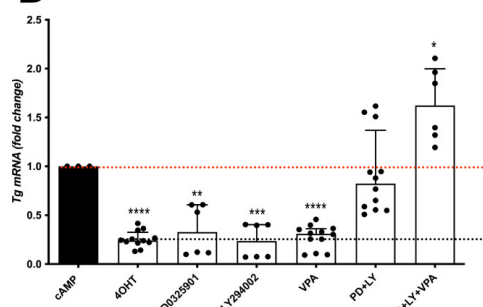
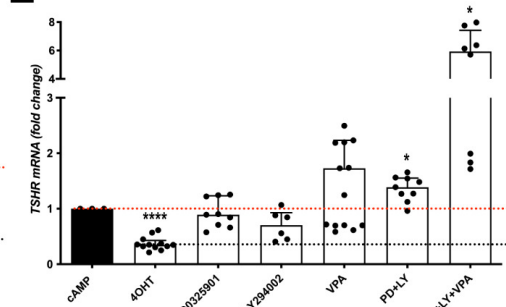
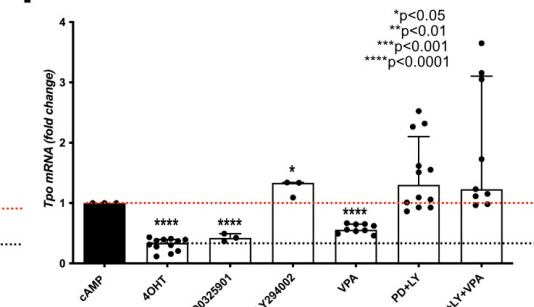
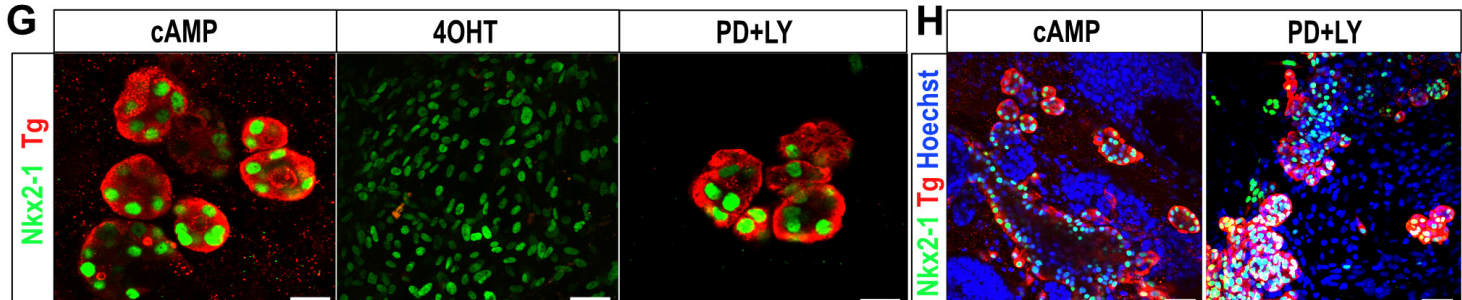
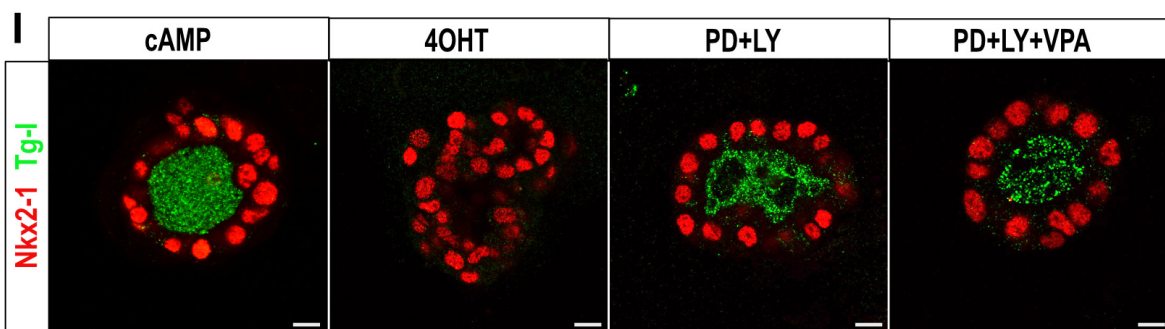
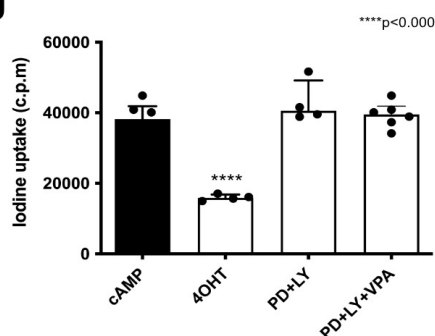
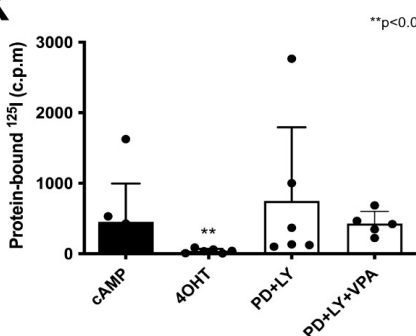
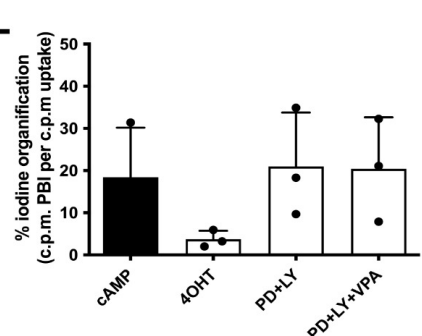
1161

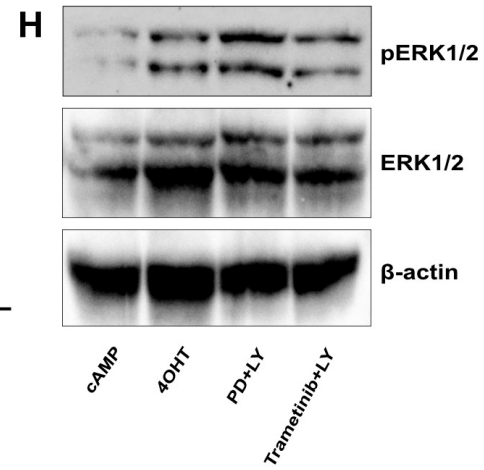
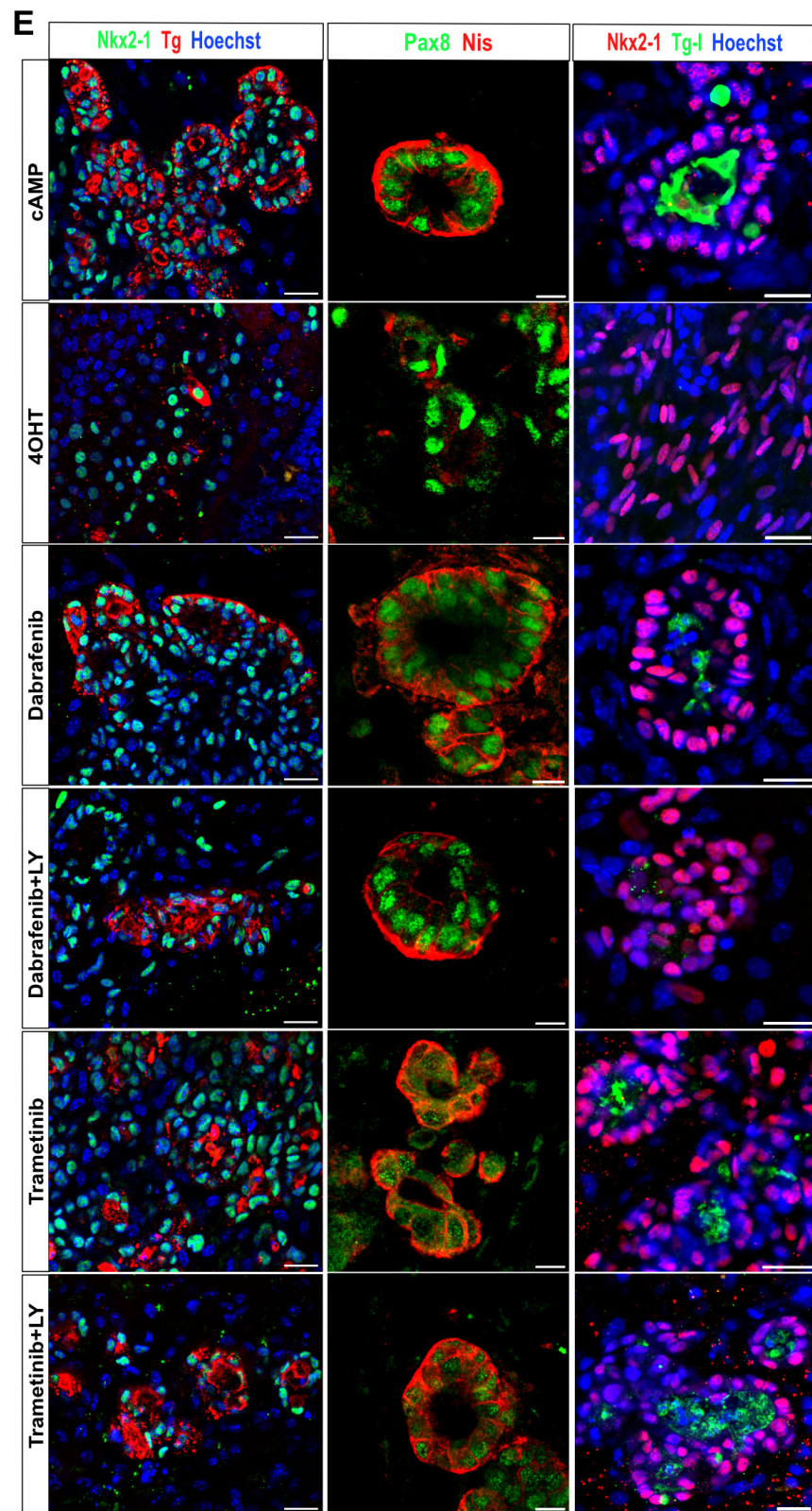
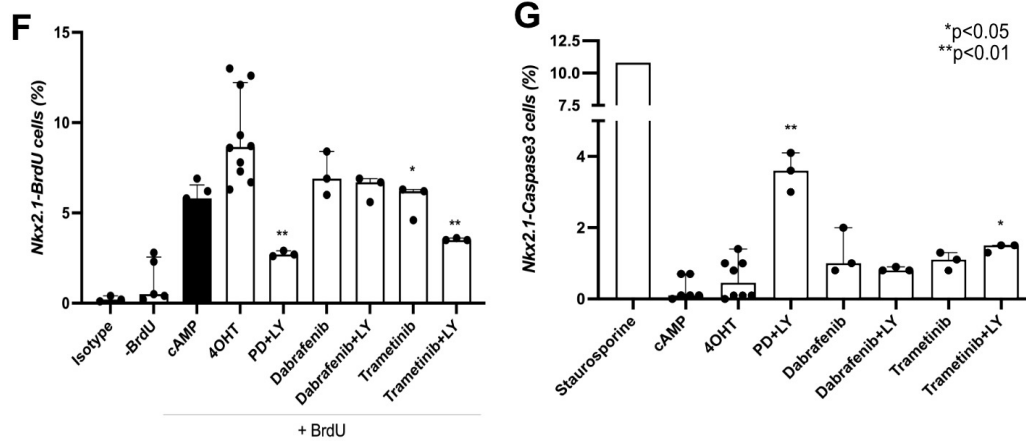
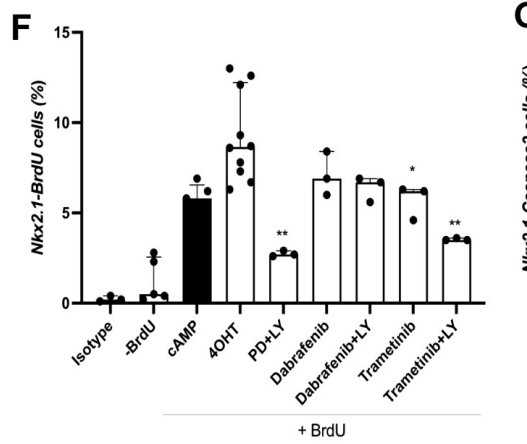
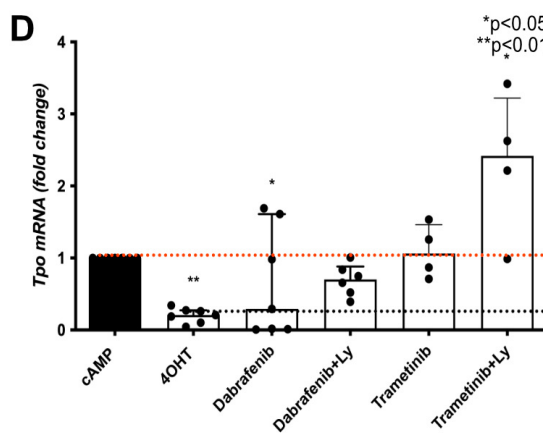
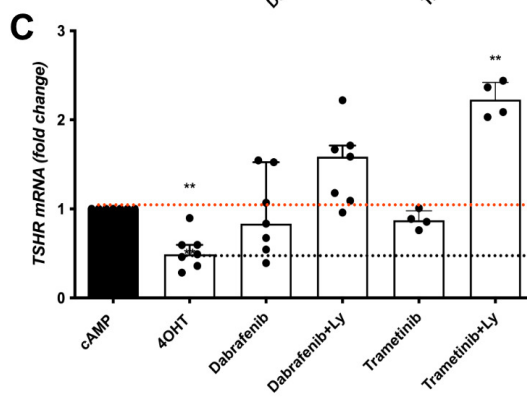
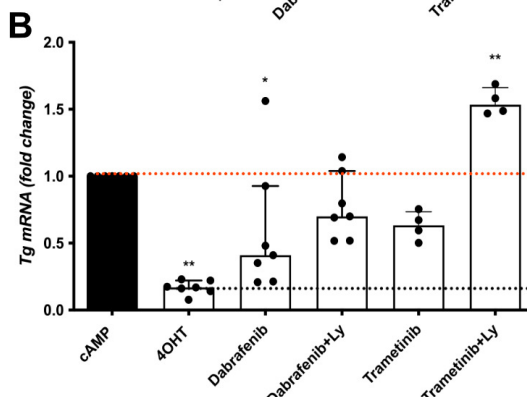
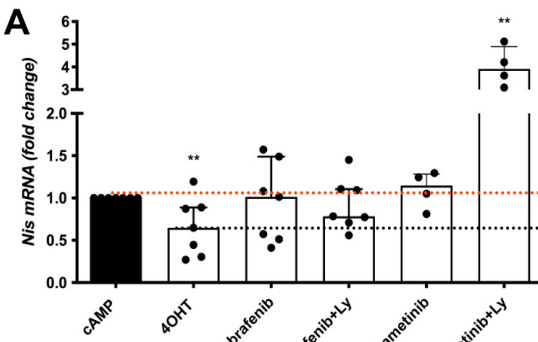
1162 **Fig. 6 Transcriptomics analysis confirms thyroid redifferentiation of Braf^{V637E}-**
1163 **expressing cells treated with MAPK and PI3K inhibitors and suggests by which**
1164 **mechanisms.** Heatmap of normalized bulk RNA-Seq expression of normal thyroid cells
1165 (cAMP), Braf^{V637E} expressing cells (4OHT), and Braf^{V637E} expressing cells treated with
1166 PD0325901+LY204002 inhibitors. Rows represent markers and columns represent
1167 specific conditions. Color values in the heatmap represent mean expression levels (A).
1168 Thyroid differentiation (eTDS and TDS) (B) and ERK (C) scores were calculated among
1169 the different conditions. Classification of upregulated and downregulated genes
1170 comparing 4OHT *vs.* cAMP (D, E) and PD+LY *vs.* 4OHT (F, G). Colors represent the
1171 classification method and scale the -log10 (adj p-value).

A**B****E****C****F****D****G**



A**Nkx2-1 Tg Hoechst****Nkx2-1 Tg****E-Cadh Nkx2-1 Hoechst****Zo-1 Nkx2-1 Hoechst****Nis Nkx2-1****Tg-I Nkx2-1 Hoechst****G****Nkx2-1 Tg Hoechst****H****Nkx2-1 Tg Hoechst**

A**B****C****D****E****F****G****H****J****K****L**



Upregulated genes

Downregulated genes

